Universidade Federal do ABC

ACTIVATION UNDER VISIBLE LIGHT OF STRONTIUM TITANATE SURFACE FOR WATER SPLITTING INTO HYDROGEN AND OXYGEN MOLECULES.

SWAGOTOM SARKAR

SANTO ANDRÉ

2017

Universidade Federal do ABC

ACTIVATION UNDER VISIBLE LIGHT OF STRONTIUM TITANATE SURFACE FOR WATER SPLITTING INTO HYDROGEN AND OXYGEN MOLECULES.

SWAGOTOM SARKAR

DISSERTATION PRESENTED IN PARTIAL FULFILMENT OF THE REQUIREMENTS OBTAIN MASTER DEGREE IN NANOSCIENCES AND ADVANCED MATERIALS

SUPERVISOR:

PROF. DR. FLAVIO LEANDRO DE SOUZA

CO-SUPERVISOR:

PROF. DR. SYDNEY FERREIRA SANTOS

SANTO ANDRÉ

2017

MINISTÉRIO DA EDUCAÇÃO
Fundação Universidade Federal do ABC
Programa de Pós-Graduação em Nanociências e Materiais Avançados
Avenida dos Estados, 5001 – Bairro Santa Terezinha – Santo André – SP
CEP 09210-580 · Fone: (11) 4996-0017
pgp.nanomat@ufabc.edu.br

FOLHA DE ASSINATURAS

Assinaturas dos membros da Banca Examinadora que avaliou e aprovou a Defesa de Dissertação de Mestrado do candidato Swagotom Sarkar, realizada em 14 de fevereiro de 2017:

Prof.(a) Dr.(a) **Sydney Ferreira Santos** (Universidade Federal do ABC) Presidente

Prof.(a) Dr.(a) **Jeverson Teodoro Arantes Junior** (Universidade Federal do ABC) – Membro Titular

Prof.(a) Dr.(a) **Jean Jacques Bonvent** (Universidade Federal do ABC) – Membro Titular

Prof.(a) Dr.(a) **Fabio Furlan Ferreira** (Universidade Federal do ABC) – Membro Suplente

Prof.(a) Dr.(a) **Leticie Mendonça Ferreira** (Universidade Federal do ABC) – Membro Suplente

Este exemplar foi revisado e alterado em relação à versão original, de acordo com as observações levantadas pela banca no dia da defesa, sob responsabilidade única do autor e com a anuência de seu orientador.

Santo André, 20 **de** abril **de 20**17**.**

Assinatura do autor: _____

Assinatura do orientador: _____

FINANCIAL SUPPORT:

I am very grateful to the CNPQ scholarship program which allowed me to study on my dream subject – Nanoscience and Advanced Material for my master degree here at UFABC, Santo Andre, SP , Brazil.

ACKNOWLEDGEMENTS

I am very much acknowledged to Lord Krishna for giving me such a great opportunity to study such a great university – UFABC, Santo André, SP, Brazil.

I am very much thankful to my supervisor for selecting me as his research student.

I also would like to appreciate the amicable help which I got from Waldemir, André, Dete, Aryane, Daniel and Victoria.

I would like to acknowledge financial support from Brazilian agencies CEPID/CDMF FAPESP (2013/07296-2) and CNPq.

Finally, I am very much grateful to my parents for their encouragement to come abroad for my higher studies.

RESUMO

Titanato de estrôncio é um material semicondutor interessante para aplicação em células fotoeletroquímicas. Uma via simples e de baixo custo para a preparação de fotoeletrodos de titanato de estrôncio é o método sol-gel. O método complexo polimerizado permite um controle ótimo da estequiometria e da incorporação de dopantes durante o processo. Neste trabalho, fotoanodos de titanato de estrôncio puro e dopado foram preparados usando o método sol-gel. Em primeiro lugar, fotoanodos de titanato de estrôncio puro foram produzidos e tratados termicamente a 800 °C. Em seguida, incorporaram-se os dopantes de ítrio (Y^{2+}) e níquel (Ni^{2+}), sendo realizado uma otimização de deposição para alcançar o melhor desempenho fotoeletroquímico. Além disso, avaliou-se a influência de um tratamento térmico em diferentes condições atmosféricas (nitrogênio e oxigênio) nas propriedades fotoeletroquímicas. Todos os fotoanodos foram analisados estruturalmente, morfologicamente e eletro/fotoeletroquimicamente. As deposições de 6 camadas e 4 tratamentos térmicos de puros e dopados, exibiram a melhor performance analisada por voltametria de varredura linear. Destacou-se os fotoanodos dopados com ítrio, apresentando a maior fotocorrente, comparado com o puro e o dopado com níquel. Adicionalmente, foram analisadas as contribuições na atividade catalítica favorecida pelo tratamento térmica adicional de 15 minutos em atmosfera rica e deficiente em oxigênio. Observou-se que o desempenho aumentou para o material puro submetido a um tratamento térmico adicional em atmosfera de oxigênio e para material dopado com ítrio e submetido a tratamento em atmosfera de nitrogênio. No entanto, fotoanodos de titanato de estrônico, nas diferentes condições de síntese e atmosfera de tratamento térmico, apresentam o desempenho fotoeletroquímico baixo. Em primeiro lugar, o intervalo de banda de titanato de estrôncio puro é muito elevado, 3,2 eV, que permite absorver uma pequena faixa do espectro da radiação solar. Por fim, sugere-se que a maior parte dos dopantes podem estar segregando nos contornos, podendo atuar como centros de recombinação, que reduz a eficiência das reações de superfície. Finalmente, os fotoanodos foram analisados eletroquimicamente através de espectroscopia impedância eletroquímica (EIS) para analisar os possíveis limitantes na performance do material.

Palavras-chave: Titanato de estrôncio, fotoanodos, dopagem, desempenho fotoeletroquímico.

ABSTRACT

Strontium titanate is an interesting semiconductor to be applied in photoelectrochemical cells. A simple and cost effective route to prepare strontium titanate photoelectrode is the sol-gel method. The polymerized complex method allows an optimal control of stoichiometry and the incorporation of impurities during the process. In this work, pure and doped strontium titanate photoanodes were prepared by using sol-gel method. Firstly, pure strontium titanate films were produced and heat treated at 800°C. Then, yttrium (Y^{2+}) and nickel (Ni^{2+}) dopants were incorporated. It was made a deposition optimization in order to achieve the best photoelectrochemical performance. Additionally, it was evaluated the influence of an extra heat treatment at different atmosphere (nitrogen and oxygen) on photoanodes properties. All the photoanodes were analyzed structurally, morphologically and electro/photoelectrochemically. Pure and doped strontium titanate photoanodes with 6 layer depositions and 4 time heat treatments exhibited best photocurrent than other conditions provided by linear sweep voltammetry. Yttrium-doped exhibited best photocurrent than pure and nickel-doped strontium titanate. Finally, catalytic activity of pure strontium titanate with extra heat treatment for 15 minutes in oxygen atmosphere and yttrium-doped strontium titanate with extra heat treatment for 15 minutes in nitrogen atmosphere was increased. Nevertheless, photocurrent performances of pure and modified strontium titanate films under air, nitrogen, oxygen atmosphere was very poor which can be explained by plausible hypothesis. Firstly, the band gap of pure strontium titanate is very high – 3.2 eV. So, It only absorbs UV light which is only 4% of sun light. Secondly, most of the dopants may be segregated which may act as recombination centers that reduced the charge separation efficiency. Finally, polaron size of pure and doped strontium titanate under extra oxygen atmosphere decreases. Thus, resistance to charge transfer increases. Under extra nitrogen atmosphere, recombination may have increased as these films exhibited higher conductivity than films prepared under oxygen atmosphere.

Keywords: Strontium titanate, photoanodes, dopants, photoelectrochemical performance

FIGURES:

Figure 1: Primitive phase diagram for hydrogen.....2

Figure 2: Photo electrochemical cell to split water molecule into hydrogen fuel…….....3

Figure 3: Relative positions of various semiconductor conduction band and valence in aqueous electrolyte at pH 7..…….....5

Figure 4: Pechini method sequence for the preparation of metal oxides…….…….....7

Figure 5 : Atomic structure of SrTiO3 at room temperature…….9

Figure 6 : Schematic procedure to prepare solution…….....13

Figure 7: Solution image for (a) pure SrTiO3 and (b) Y doped SrTiO3…….....14

Figure 8: Schematic procedure for film preparation…….....16

Figure 9: Image of the prepared thin films pure and Y-doping STO…….....19

Figure 10: XRD patterns of Strontium titanate thin films deposited on FTO glass substrate after thermal heat treatment…….....19

Figure 11: TOP view SEM image of STO and YSTO thin films a) STO 1 , b) STO 2 3 c) YSTO 1, d) YSTO 2 3, e) YSTO 4 6 thin films…….....20

Figure 12: UV-VISIBLE spectroscopy showing the change in transmittance spectra depending on the layers of each STO and YSTO photoanodes ……..….....21

Figure 13: Linear sweep graph of STO and YSTO samples under front side illumination……...22

Figure 14: Chronoamperometry showing the stability of each STO and YSTO samples under front side illumination…….....23

Figure 15: Cyclic voltammetry measurement graph for STO and YSTO samples A) STO 1, B) YSTO 1 , C) STO 2 3, D) YSTO 2 3, E) STO 4 6 , F) YSTO 4 6 thin films…….....24

Figure 16: Electrochemical Impedance Spectroscopy measurement for STO and YSTO photoanodes synthesized in different deposition and heat treatment times …….....25

Figure 17: Mott- Schottky plot for all photoanodes synthesized. For this measurement, the same a three-configuration cell and electrolyte was used. The linear adjust was done at frequency of 10 kHZ…….....26

Figure 18: X-ray diffraction study of pure and Y doped STO 4 6 thin films on FTO substrate. Asterisks (∗) indicate peaks associated with F: SnO_2 on glass substrate…….....28

Figure 19: UV – Visible spectroscoy of (a) STO 4 6 and YSTO 4 6 at air , O_2 , N_2; (b) STO 4 6 at air, O_2, N_2 and NiSTO 4 6 at air, N_2 atmosphere. Undoped STO 4 6 samples added in both graphs for better comparison…….....30

Figure 20: a) linear sweep voltametry of STO 4 6 and YSTO 4 6 prepared all in air , O_2 and N_2 atmosphere. b) linear sweep voltametry of STO 4 6 and YSTO air , O_2 and N_2 and NiSTO 4 6 at air , N_2 atmosphere …….....32

Figure 21: Chronoamperometry study of (a) STO 4 6 and YSTO 4 6 at air, N_2, O_2 atmosphere; (b) STO 4 6 at air, O_2 , N_2 and NiSTO 4 6 at air , N_2 atmosphere …….....34

Figure 22: Eletrochemical Impedance spectroscopy analysis of STO 4 6, NiSTO and YSTO 4 6 prepared at air, O_2, N_2 atmosphere. (a) STO 4 6 and YSTO 4 6; (b) STO 4 6 at air, N_2, O_2 and NiSTO 4 6 air, N_2 atmosphere. In both plot the STO was included for better comparison…….....35

Figure 23: (a) Mott-Schottky analysis of STO 4 6 and YSTO 4 6 at air,O_2, N_2 atmosphere; (b) Mott-Schottky analysis of STO 4 6 at air, N_2, O_2 and NiSTO 4 6 at air, N_2 atmosphere…….....36

TABLES:

Table 1: Physics properties of $SrTiO_3$…….....8

Table 2: Values of ionic radius , crystal structure, electronegativity and valance of Sr, Y, Ti and Ni atoms to form substitutional solid solution……..12

Table 3: Details of sample preparation and abbreviation names…….....15

Table 4: Details of samples prepared 6 times deposition and 4 times heat treated and submitted an extra heat treatment in N_2 and O_2 gas flux…….....17

Table 5: Lattice parameter of pure and Y-doped STO thin films…….....20

Table 6: Showing the current density values of each STO and Y doped STO thin films….....23

Table 7: The estimated donor density values from Mott-Schottky data…….....26

Table 8: Lattice parameter (*a*) and cell volume (*V*) calculated from XRD patterns for STO pure and Yttrium-doped in different atmospheres compared to a crystallographic standard card for cubic structure. In addition, it is showed the preferential orientation (P.O.) and crystallite size for all samples…….....28

Table 9: Calculated donor density (N_D) of STO 4 6, YSTO 4 6 and NiSTO 4 6 with different atmospheres (air, O_2 and N_2)…….....29

Summary

1. INTRODUCTION 1

1.1 Green Climate 1

1.2 Sustainable Energy Sources 1

1.3 Photoelectrochemical Cell 2

1.4 Material Requirements to be used as Photoanode 3

1.5 Polymerized Complex Method 5

1.6 $SrTiO_3$ characteristics to be applied as photoanode 7

2. OBJECTIVE 13

2.1 General 13

2.2 Specific 13

3. EXPERIMENTAL PROCEDURE 14

3.1 Methodology for pure and doped $SrTiO_3$ photo anodes 14

3.2 Characterization 18

4. RESULTS 19

4.1 Pure and Y-doped STO photoanodes: deposition optimization 19

4.2 $SrTiO_3$ best synthesis condition 27

4.2.1 Optical, structural and morphological properties for pure and doped STO 4 6 thin films heat treated at different atmospheres 27

4.2.2 Electro/Photoelectrochemical performances 31

5. CONCLUSION 37

6. REFERENCES 39

1. INTRODUCTION

1.1 Green Climate

Long-term, sustainable energy economy is the current issue of our present age. Although we have the technology and sufficient fuel reserves to provide the energy needed for centuries' but, the use of this fossil fuel is forcing us towards the doomsday [1]. It is well known that the combustion of fossil fuel produces green house gas as CO_2 which is making our earth hot. Thus, polar ice is melting and consequently, sea level is rising. If this is going on, many countries around coastal areas will go down the sea. So, it can cause destructive erosion, flooding of wetlands, contamination of aquifers and agricultural soils, and lost habitat for fishes, birds, and plants [2]. So, we need to make our environment green to halt being extinct ourselves.

1.2 Sustainable Energy Sources

To save our planet from the doomsday, we need to use sustainable energy which does not produce any greenhouse gases. There are several renewable energy sources like wind, hydroelectric, tidal and ocean current, geothermal, bio mass, nuclear and solar energy. Among them, solar energy is the only source that has the potential to meet all our energy needs. As the energy from sun is abundant many different ways of energy production can be developed. Exploiting materials able to absorb sunlight irradiation transforming it into chemical energy has been received considerable attention. Nowadays, the most promise solar fuel is hydrogen that provide highest gravimetric energy density (143MJ/KG) in comparison with any other available chemical fuel [3,4]. There are several routes to produce hydrogen from water, which are follows [1, 5, 6]:

- Photoelectrochemical water splitting
- Photocatalytic water splitting
- Coupled photovoltaic – electrolysis systems
- Thermochemical conversion
- Photobiological methods
- Molecular artificial photosynthesis
- Plasma-chemical conversion
- Mechano-catalytic, magnetolysis, radiolysis, etc

Among all the methods to generate hydrogen from solar irradiation, photoelectrochemical water splitting has been considered cheapest, and directly way to produce hydrogen fuel. Indeed, the reason behind this effort to find way to store solar irradiation into chemical fuel is due to the intermittency of sunlight. There are two types of variations, the daily variations, meaning the difference between day and night, and the seasonal variations, because the sun's irradiation in the winter is not the same as in the summer. But even if there is no sun, it is expected that the need for energy will always be covered.

Actually, the biggest problem in the current energy scenario is not the production of renewable energy, but its storage. The energy can be stored chemically. Chemical energy is the energy which comes from the energy of outer shell unpaired electrons. Hydrogen is very promising because of its electron is accompanied by only one proton. That's means highest ratio of valence electrons to protons of all the elements in the periodic table. The energy gain per mass of hydrogen (39.4 KWh/kg) is three times larger than other types of chemical fuel , for instance, liquid hydrocarbons (13.1 KWh/kg) .[60] In other words, energy of 0.33 kg of hydrogen is equal to the energy of 1 kg oil. The energy content of fuel is called heating value. The lower and upper heating values of hydrogen are 33.3 KWh-kg^{-1} and 39.4 KWh-kg^{-1}.[60]

Hydrogen molecules exist at different forms at different temperature and pressure. Hydrogen is solid with density of 70.6 $kg.m^{-3}$ at temperature -262 °C . On the other hand, hydrogen is gas with a density of 0.089886 $kg.m^{-3}$ at higher temperature (0 °C) and pressure 1 bar. Liquid hydrogen also exists with a density of 70.8 $kg.m^{-3}$ at -253 °C. It is gas at ambient temperature(298K).[60] If hydrogen is produced by using only renewable sources such as solar light or using electricity generating by wind power or hydro power, then , hydrogen is a renewable fuel. That's why, the concept of solar fuels is interesting and being discussed here[7].

1.3 Photoelectrochemical Cell

A conventional photoelectrochemical cell (PEC) is constituted by a photoanode, a counter electrode and electrolyte. PEC chemical process involves the water splitting into hydrogen and oxygen molecules using photon energy which comes from sunlight. The produced hydrogen is a form of chemical energy. Fig 1 shows a schematic approach for a PEC device.

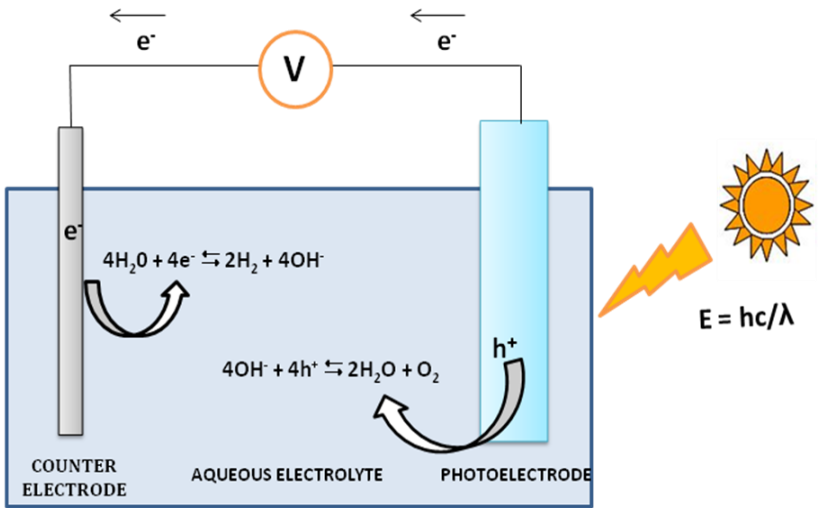

Fig 1 - Photoelectrochemical cell for water splitting into hydrogen and oxygen molecule adapted from [8].

A photoanode uses light to produce an electrochemical reaction. In this process, the photons reach the surface of this photoelectrode which is made of a photoactive semiconductor. As in any other semiconductor, the photons with the same or higher energy than the semiconductor band gap energy create an electron-hole pair. The electrons and holes will be separated by an electric field, and both will be used in the two half reactions involved in the overall water splitting process. The reaction of water splitting is a reduction-oxidation reaction, or how they are commonly known, a redox reaction.

In redox reactions, the reaction happens due to the exchange of electrons between elements or molecules.[7]

1.4 Material Requirements to be used as Photoanode

Firstly, the semiconductor used as photoanode has to absorb enough incident sunlight. Secondly, charge carrier transport inside the material and separation of the charge carrier into the two electrodes must be efficient. Thirdly, because of the overpotential, a bandgap of 1.23 eV is not sufficient to drive the reaction. It has been calculated that materials having energy band gap close to 2.1 eV have enough potential to split water. Fourthly, energy levels of the photoanode or photocathode materials must be adequate to couple with the potential needed for the reaction.

The potential of the reactions must be located somewhere in the energy band gap of the semiconductor, which is called the favorable position. To further enhance the reaction, a catalyst may be added to the semiconductor surface. On the practical side, it is very important

that the photoanode or photocathode materials are photo electrochemically stable and relatively cheap. [7]

There are several metal oxides like: TiO_2[10,11,12,13], WO_3[14,15,16], ZnO[17], CuO[18] and α-Fe_2O_3[19,20,21,22] which have been used as photoanodes in photoelectrochemical cells to produce hydrogen. The main requirements in a PEC is that the semiconductor conduction band limit has to be relatively more negative than the water reduction potential, while the valence band limit has to be relatively more positive than the water oxidation potential.We can explain this following way – at the photostationary state(semiconductor under light condition), the concentration of electrons and holes alters. As a result, an individual Fermi level for electrons and holes can be defined at this state. This Fermi level is called quasi Fermi level [57] because there is no thermal equilibrium. The quasi Fermi level is the driving force for charge transfer reaction.

The movement of electrons from the conduction band to oxidant particles is only possible if Fermi level of the electrons is greater than the Fermi level of oxidant particles (Equation 1).

$$E_{Fn} > E_{F\,(redox)} \tag{1}$$

Similarly, the transfer of holes from the valence band to oxidant particles is possible if the fermi level of holes is lower than the Fermi level of reductant particles (Equation 2).

$$E_{Fp} < E_{F\,(redox)} \tag{2}$$

By considering the above relationship, the thermodynamic condition for electrolysis of water is:

$$E_{Fn} > E_{F\,(H^+/H_2)} \tag{3}$$

$$E_{Fn} > E_{F\,(O_2/H_2O)} \tag{4}$$

That is why band edge positions of semiconductor relative to conduction and valence potential of water are the main requirements for the electrolysis of water.[8] We can use the following Fig 2 to get it understand clearly.

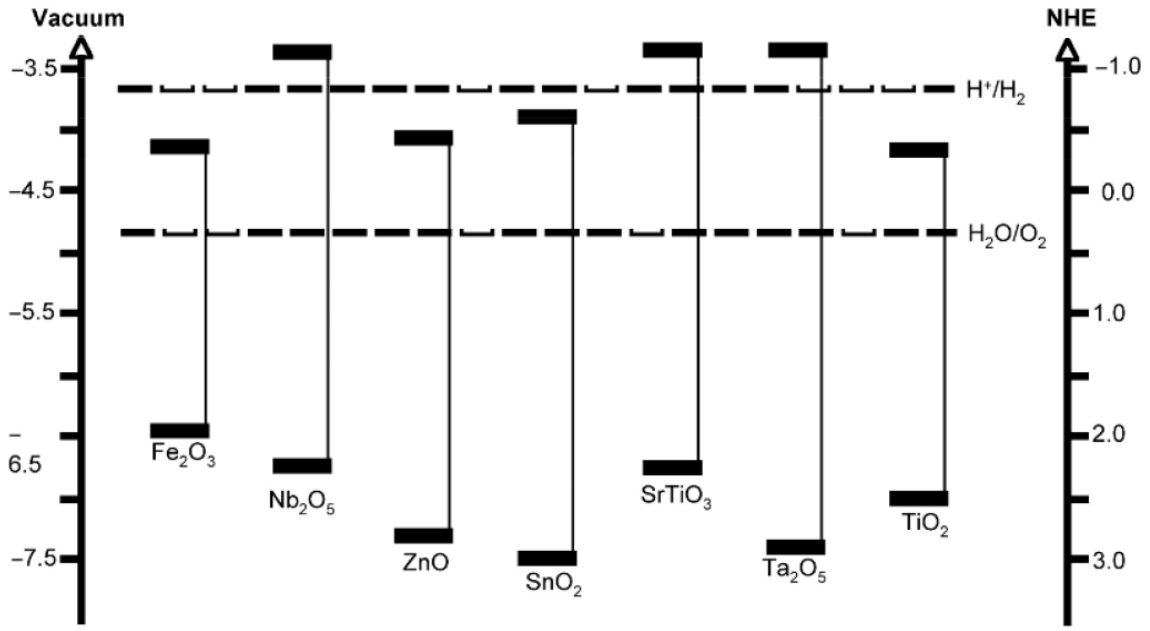

Fig 2 -Relative positions of various semiconductor conduction band and valence in aqueous electrolyte at pH 7. Adapted from reference [23].

It has been seen from the Fig 2 that most of these materials have conduction band close to or more positive than water reduction potential. So, those materials are not of good choice to produce hydrogen, spontaneously. In this case, $SrTiO_3$ is a material which has the conduction band more negative than water reduction potential. That means, it is not necessary to apply an external bias to generate hydrogen in case of $SrTiO_3$ photoanode material. Applying all those concepts associated with photoanode, we have been produced at Universidade Federal do ABC different photoanode such as: ZnO, WO_3, Fe_2O_3 and $SrTiO_3$.

1.5 Polymerized Complex Method

$SrTiO_3$ photoanodes have been prepared with different morphology by various methods such as: solution phase decomposition [24], ultrasonic chemical method.[26] Among of them, sol-gel method has been considered a most promise route to prepare $SrTiO_3$ thin film with two main advantages: a) homogeneous and stoichiometric compounds and b) low processing cost . The method starts with a molecular precursor, which passes through two chemical stages: the formation of colloidal particles in a liquid phase (sol), which then turn into a three-dimensional network (gel).

Metal oxide films can be obtained by the successive deposition of the sol-gel on a substrate and an adequate heat treatment. Metal alkoxides are one type of precursor used in

technique. Metal alkoxides undergo hydrolysis and condensation when in contact with water (sol). In the hydrolysis reaction, OH groups bounded to the metal are formed, while in the condensation these hydrolyzed monomers can react to form metal-oxygen-metal bonds. These bonds are formed either by the reaction of two hydrolyzed monomers or by the reaction of a hydrolyzed monomer and the metal alkoxides. Inorganic polymers (gel) are, thus, formed by a progressive condensation.

$$-M-OR \;+\; H_2O \;\rightarrow\; -M-OH \;+\; ROH \tag{5}$$

$$-M-OH \;+\; HO-M- \;\rightarrow\; -M-O-M- \;+\; H_2O \tag{6}$$

$$-M-OR \;+\; HO-M- \;\rightarrow\; -M-O-M- \;+\; ROH \tag{7}$$

There are two other kinds of methodologies that do not fit strictly into the previous sol-gel process but are also considered sol-gel techniques. These routes are the polymerized complex method (PC) and the polymer precursor method (PP) which involve the presence of organic polymers acting as the gel. Metal cations are stabilized by coordinating organic polymers that can be formed in situ or not. In the polymer precursor method, a viscous solution is prepared by mixing an adequate polymer and metal oxide precursor in a suitable solvent. The polymerized complex method refers to the coordination of the metal ion by a chelating molecule that simultaneously undergoes polymerization.[27]

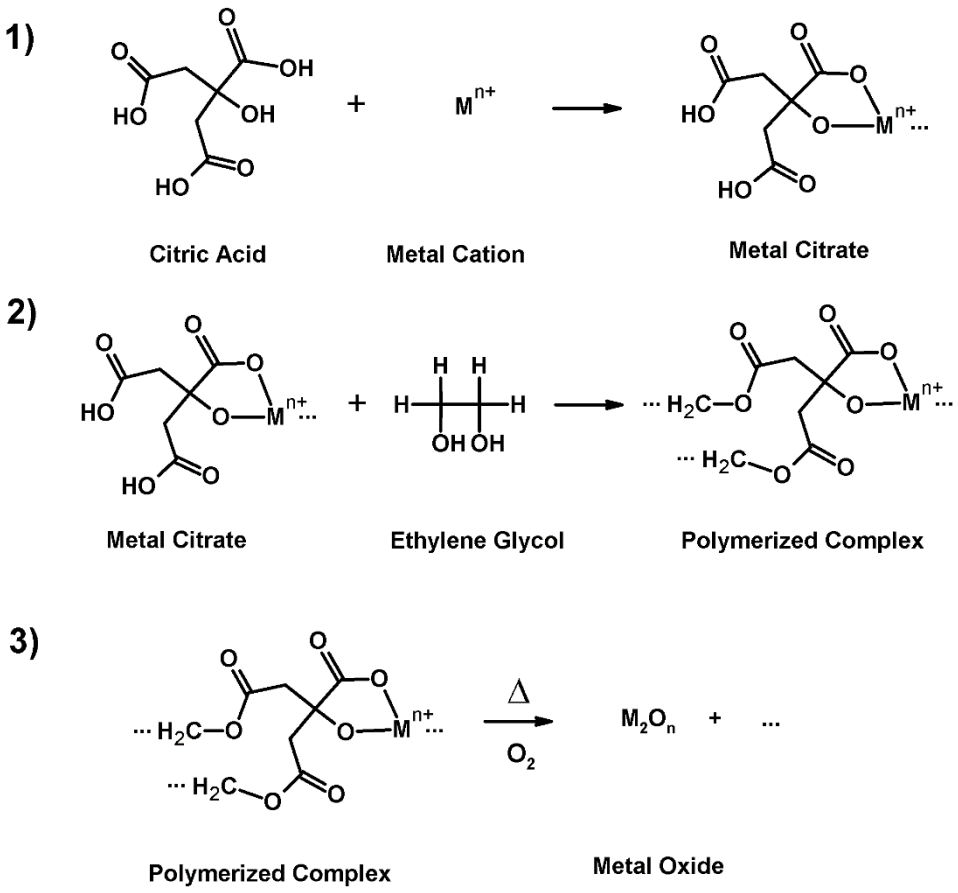

Fig 3 - Pechini method sequence for the preparation of metal oxides.

The Pechini method is an example of the PC method (Fig 3). This method uses a polycarboxylic acid and a polyalcohol as precursors for the polyesterification reaction. Citric acid and ethylene glycol are commonly used as the polycarboylic acid and polyalcohol, respectively, to form the polymer network. Citric acid has three carboxyl groups and has been used because it stabilizes non-monovalent metal cations very well.

1.6 $SrTiO_3$ characteristics to be applied as photoanode

In the last decade, an intense effort has been done for developing efficient materials to store sunlight irradiation into chemical energy. Fujjishima and Honda showed in 1972 for the first time how to store solar energy into oxygen and hydrogen fuel by splitting water molecule using TiO_2 photoanode.[28] From there, several semiconductors like Fe_2O_3, WO_3, ZnO and $BiVO_4$, for example, have been studied to be applied as photoanode in photoelectrochemical devices. These oxide semiconductors show high photocurrent but they have a large drawback

that they need a large overpotential to split water molecule. In this case, $SrTiO_3$ rise as a promising candidate in photoelectrochemical conversion of sunlight into hydrogen fuel [25].

Perovskites are good candidates for anode materials because it is known to possess properties such as high electronic conductivity, high oxide ion conductivity and good catalytic activity. $SrTiO_3$ is a n-type photoanode with high photochemical and chemical stability and band gap energy of 3.2eV. This $SrTiO_3$ photoanode was considered as a promising photoanode in 1970s.[28] Most recently, Leite and co-workers [25] reported high photocurrent using Nb doped $SrTiO_3$ photoanode. $SrTiO_3$ can also be doped by La^{3+} on the site of Sr^{2+} and Nb^{5+} on the site of Ti^{4+} which will convert $SrTiO_3$ into highly conducting n-type material, on the other hand, if STO is doped by Fe^{3+} and Al^{3+} on the site of Ti^{4+} a p-type material will be produced.[29,30] Xue Li´s group [31] reported that Y doped $SrTiO_3$ anode can increase electrical conductivity when Y amount is less than 0.09 in $Y_xSr_{1-x}O_3$. So, we wanted to investigate photoelectrochemical properties of Y doped $SrTiO_3$ to split water molecule into hydrogen fuel. Table 2 presents the physics properties for $SrTiO_3$.

Table 1. Physics properties of $SrTiO_3$

Property	Value
Atomic density	5.12 g/cm^3
Melting point	2080 °C
Dielectric constant (ε_0)	200
Thermal conductivity	12 W/mK
Coefficient of thermal expansion	9.4 $x10^{-6}$ Å/°C
Refractive index	2.31- 2.38

$SrTiO_3$ crystallizes in the ABO_3 cubic perovskite structure at room temperature and atomic structure for this material is showed in Fig 4.

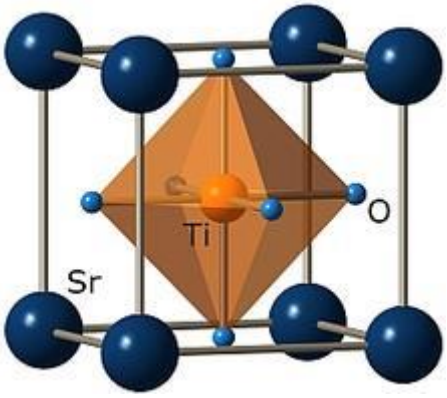

Fig 4 - Atomic structure of SrTiO3 at room temperature. [32]

This material has space group Pm3m with lattice parameter of 0.3905 nm and density of ρ = 5.12 g/cm^3. The Ti^{4+} ions are sixfold coordinated by O^{2-} ions and each Sr^{2+} ions are surrounded by four TiO_6 octahedra. Therefore, each Sr^{2+} ion is coordinated by twelve O^{2-} ions.[33] Hybridization between 2p orbital of oxygen and 3d orbital of titanium produces covalent bonding within TiO_6, on the other hand, Sr^{2+} and O^{2-} ions give rise to ionic bonding character.[34] So, $SrTiO_3$ has mixed ionic-covalent bonding properties. This nature of chemical bonding makes it a model electronic material.

If cation dopant is introduced in the lattice, distortion from cubic to lower symmetrics is occurred.A distortion from cubic to lower symmetries occurs on lower temperature or in a presence of cation-dopant introduced in the lattice (e.g. ion implantation). Distortions are related to three main effects: size effects, deviations from the ideal composition and the Jahn - Teller effect.

Crystallographic distortion degree to accommodate different size cations shown by most perovskites can be predicted by the Goldschmidt criterion.[35] Tolerance factor (t) of the perovskite-type ABO_3 can be defined as follows:

$$t = \frac{r_A + r_O}{\sqrt{2}(r_B - r_O)} \tag{8}$$

where r_A is the ionic radius of atom A, r_B is the ionic radius of atom B, and r_O is the ionic radius of oxygen. The ideal cubic perovskite $SrTiO_3$ has t = 1, r_A = 1.44 Å, r_B = 0.605 Å and r_O = 1.40 Å.

However, if t shows a deviation from l, this might indicate the formation of a perovskite structure of non-ideal type, which is predicted for $0.89 < t < 1$. The tolerance factor value becomes smaller than 1 if A ion is smaller than the ideal value or if B ion is too large.

For example, $CaTiO_3$ with t = 0.82 is orthorhombic. On the other hand, if tolerance factor value is larger than 1, then tetragonal and hexagonal variants of the perovskite structure are stable, e.g. $BaTiO_3$ (t = 1.062) and $BaNiO_3$ (t = 1.13) type structures. In these cases, close packed layers are stacked in tetragonal and hexagonal manners in contrast to the cubic one formed for $SrTiO_3$.[36]

Since perovskites are not truly ionic compounds and values are taken for the ionic radii, the tolerance factor is only a rough estimation giving an indication for compounds with a high degree of ionic bonding. The distortions exhibited by perovskites, because of cation substitution, can be used to fine tune and adjust properties of interest. Some of these include conductivity, dielectrics, and colossal magnetoresistance.

Many ABO_3 perovskites with reducible B cations can form vacancy ordered superstructures of general formula $A_nB_nO_{3n-1}$. That is, oxygen deficient perovskites may be formed if the valence of the B cation can be changed either by heat treatment in oxidizing/reducing atmospheres or via doping in the A sub-lattice. The oxygen vacancies are ordered preferentially with respect to local structure, i.e. octahedral, square pyramidal, tetrahedral or square planar coordination.[37]

An example, it is the family of compounds $SrFeO_n$ ($2.5 \leq n \leq 3$). The valence of Fe ions can be changed by heating in oxidizing / reducing environment. Thus, the oxygen content can vary in between 2.5 and 3. For example in $SrFeO_{2.875}$ some Fe ions can be assigned to the oxidation state +3 and others to +4. The oxygen vacancy is order, so that FeO_5 square pyramids are formed. The SrFeO compounds are examples of defect perovskites, which kept interest in them high, not only for their defect structural chemistry, but also because of two oxidation states of metallic cation.[38]

Furthermore, many oxygen deficient perovskites become good ionic conductors increasing the number of oxygen vacancies in systems like $Sr_n(Fe/Ti)O_{3n-1}$ by replacing Ti for Fe.

For electrical doping, the purpose is introducing electrically active n or p-type dopants to increase the free carrier concentration which is an important challenge for photoelectrochemical devices. The most important criterion for a possible substitution, in the case of Sr or Ti site ions by dopants which is a comparable ionic radius of the corresponding species.

The incorporation of donor and acceptor dopants into the structure leads respectively to an excess of positively or negatively charged carriers in the perovskite lattice since the

electronic states introduced within the crystal band gap by donor and acceptor impurities are either located near the valence or conduction bands thermally absorbing or injecting electrons into the material. There are some factors that needs to be considered to find out suitable dopant for a host element. Those factors to form substitutional solid solution are follows:

1. Crystal structure factor: Two atoms (dopant atom and host atom) should have same crystal structure to form complete solid solution. For instance, both atoms should have F.C.C. or B.C.C. or H.C.P. structure.
2. Relative size factor: Both atoms or elements should have atomic or ionic radius differences less than 15%.
3. Electronegativity factor: The electronegativity difference between dopant and host element should be small. Otherwise these two elements can make intermetallic compounds instead of substitution.
4. Relative valence factor: Valence should be same or nearly same.

As an example, If $SrTiO_3$ can be doped with Y and Ni to substitute Sr and Ti respectively which can be explained by following:

Although, Electronegativity and crystal structure of Sr and Y are different, Sr can be replaced by Y because Ionic radius of Sr and Y is more or less 15% with respect to each other which is in agreement with 2^{nd} rule. In addition, Valance of Sr is one unit less than Y which is in agreement with 4^{th} rule. Then, Ni can be used to replace Ti because ionic radius and electronegativity of these two elements are nearly same, although crystal structure and valance are different.

Table 2: Values of ionic radius, crystal structure, electronegativity and valance of Sr, Y, Ti and Ni atoms to form substitutional solid solution[59].

Element	Ionic radius (Å)	Crystal structure	Electronegativity	Valency
Sr	1.180	FCC	0.85	2+
Y	0.900	HCP	1.22	3+
Ti	0.605	HCP	1.54	4+
Ni	0.700	FCC	1.91	2+

Despite of all the studies performed in doped $SrTiO_3$, the rich variations in physical properties arising from carrier doping are not yet thoroughly understood. While n-type conductivity, achieved by substituting Ti^{4+} (or Sr^{2+}) for Nb^{5+} (or La^{3+}) has been found and gave rise to practical applications (e.g. electrodes and gas sensors), p-type conductivity in $SrTiO_3$ is not confirmed.[29]

Omor et al have reported that perovskite $SrTiO_3$ can act as efficient electron transporter for hybrid perovskite solar cells. [34] $SrTiO_3$ in the perovskite structure is a very attractive material for application to microelectronics because of its high charge storage capacity, good insulating properties, excellent optical transparency in the visible region and chemical stability. [39,40,41]. In the past, SrTiO3 was used as substrate for epitaxial growth of high temperature superconducting films.[42]

$SrTiO_3$ has also attracted attention in the field of carbon free energy production. The deal for this material is its poor visible light absorption. To investigate the photoelectrochemical performance for $SrTiO_3$ photoanodes, there are studies confirming that introducing doping element could increase visible light absorption. As an example, J.W.Liu et al [43] reported that Cr-doped $SrTiO_3$ photoanodes for water splitting under visible light condition. So, it is possible to split water under visible condition, if high band gap material is doped with suitable dopant.

Another important parameter for such application is the material thickness. It was reported that the energy conversion of strontium titanate photoanodes depends on its thickness with high absorption and low recombination rates optimized at 5 μm of thickness. [44]

In this work, it was studied the preparation of pure and doped $SrTiO_3$ photoanodes by using sol-gel method to apply in a photoelectrochemical cell. It was set the best deposition condition and have investigated the influence of different atmospheres on the material performance.

2. OBJECTIVE

2.1 General

The main purpose of this research project is to develop a way to make strontium titanate an efficient electrode for photoelectrocehmical application. Indeed, a shift on the absorption coefficient from UV region to visible light is an important challenge to overcome and is addressed here.

2.2 Specific

- To investigate the optimized deposition and heat treatment times for best photoelectrochemical performance by $SrTiO_3$ films;
- To prepare pure, Y-doped and Ni-doped $SrTiO_3$ films by the cost-effective sol-gel method at the best deposition condition;
- Structural, optical and morphological characterization of both pure and doped $SrTiO_3$;
- To study electrochemical and photoelectrochemical properties of pure and doped $SrTiO_3$ photoanode;
- To analyze the influence of additional heat treatment at different atmospheres (air, nitrogen and oxygen) on the electrochemical and photoelectrochemical properties for pure and doped photoanodes;

3. EXPERIMENTAL PROCEDURE

3.1 Methodology for pure and doped $SrTiO_3$ photo anodes

Undoped and modified solutions were prepared by sol-gel method as described in ref 52. To prepare the solution, at first, 1.68 ml titanium iso-propoxide was dissolved by 12.5 ml ethylene glycol with continious magnetic stirring at room temperature for 30 minutes. Then, 10.414 g citric acid was added slowly at 70°C for 2 hours. followed by addition of 0.8290 g $SrCO_3$ at constant magnetic stirring kept the temperature at 70°C for 4 hours.

After that the solution was subjected to ultrasonic vibration under room temperature for 30 minutes to guarantee the complete dispersion and homogeneity. Finally, it was kept in the refrigerator to make the solution bubble free. For ytrium-doped solution, 1% mol of doping agent Y_2O_3 was added just after the addition of $SrCO_3$ in the final stage. Fig 5 shows a schematic procedure to prepare the solution for deposition.

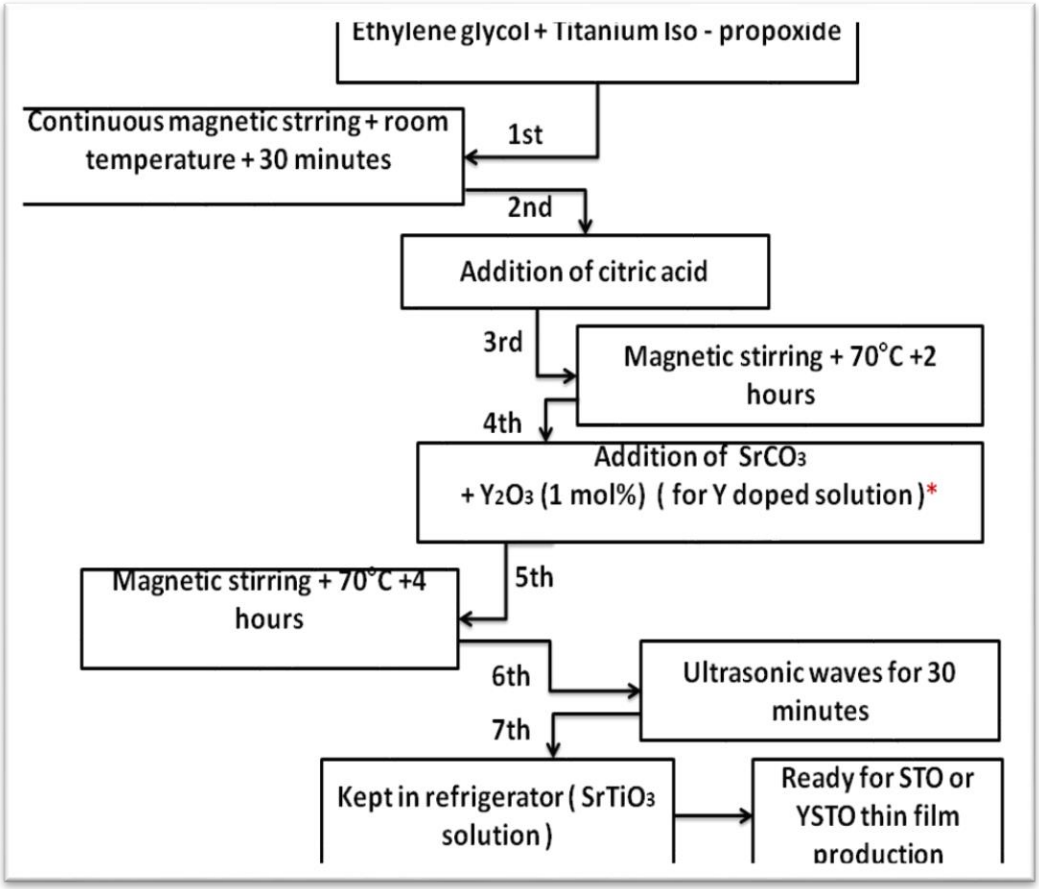

Fig 5 – Schematic procedure to prepare solution. ∗ indicates step only used for doped solution preparation.

Pure and Y-doped $SrTiO_3$ were deposited on fluorine doped tin oxide (FTO) glass substrate by dip coating method. It is worth to mention that the photoelectrode preparation was done by using the solution (Fig 6) at room temperature.

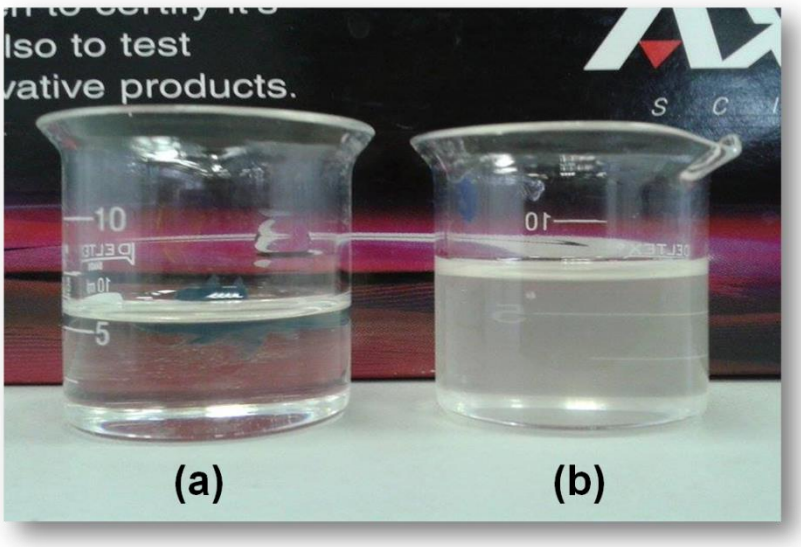

Fig 6 – Solution image for (a) pure SrTiO3 and (b) Y-doped SrTiO3.

Before the deposition process the FTO substrate was cleaned by 10 ml of *Extran* added in beaker kept at 120 °C to remove impurities from the FTO surface. Then, it was washed several times by distilled water, ethanol and dried. As mentioned before, pure and Y-doped photo-electrodes were prepared by dip coating method at room temperature with controlled withdrawn velocity at around 135 mm/min. It is the highest withdrawn speed of the dip coating machine. Substrate was immersed into the solution for 3 minutes and after dip coated substrate was kept inside dip coating machine for 1 hour and 45 minutes to guarantee a homogenous deposition and solvent evaporation. Then, it was taken out from dip coating equipment and was heated on hot plate for 15 minutes at 70 ^{o}C for better adherence and solvent evaporation.

In the first study, it was evaluated different approaches for deposition conditions. Table 3 summarized the details for photoelectrodes preparation related to deposition time and heat treatment with their abbreviation names.

Table 3 - Details of sample preparation and abbreviation names

	Characteristics	Deposition times	Heat treatment times
STO 1	SrTiO3	1 (1^{s} day = 1 time)	1 (1st day = 1 time)
YSTO 1	Y-doped SrTiO3	1 (1^{s} day = 1 time)	1 (1st day = 1 time)
STO 2 3	SrTiO3	3 (1st day = 1 time, 2nd day = 2 times)	2 (1st day = 1 time, 2nd day = 1 time)
YSTO 2 3	Y-doped SrTiO3	3 (1st day = 1 time, 2nd day = 2 times)	2 (1st day = 1 time, 2nd day =1 time)
STO 4 6	SrTiO3	6 (1st day = 1 time, 2nd day = 2 times, 3rd day = 2 times, 4th day = 1 time)	4 (1st day = 1 time, 2nd day = 1 times, 3rd day = 1 time, 4th day = 1 time)
YSTO 4 6	Y-doped SrTiO3	6 (1st day = 1 time, 2nd day = 2 times, 3rd day = 2 times, 4th day = 1 time)	4 (1st day = 1 time, 2nd day = 1 time, 3rd day = 1 time, 4th day = 1 time)

There two ways to increase layers of the photo-electrodes. One is one by one dip – coating deposition and finally heat treatment by tube furnace. Another one is one time dip coating deposition and then heat treatment. Then, use the later one procedure several times to increase layers. So, it was used hybrid procedure combining the above described procedure. The produced photo-anodes were submitted to an additional heat treatment using a tube furnace at 800 °C for 30 minutes in air. Here, 800 °C was used to anneal photo-electrodes because this temperature was confirmed as the optimized annealing temperature to prepare $SrTiO_3$ by A.N. Pinheiro et al.[25]In order to avoid any damage on the glass/layer it was used a controlled heating rate at around 3.0 °C/min and cooling rate around 1.0 °C/min. The deposition procedure steps has been shown in the Fig 7.

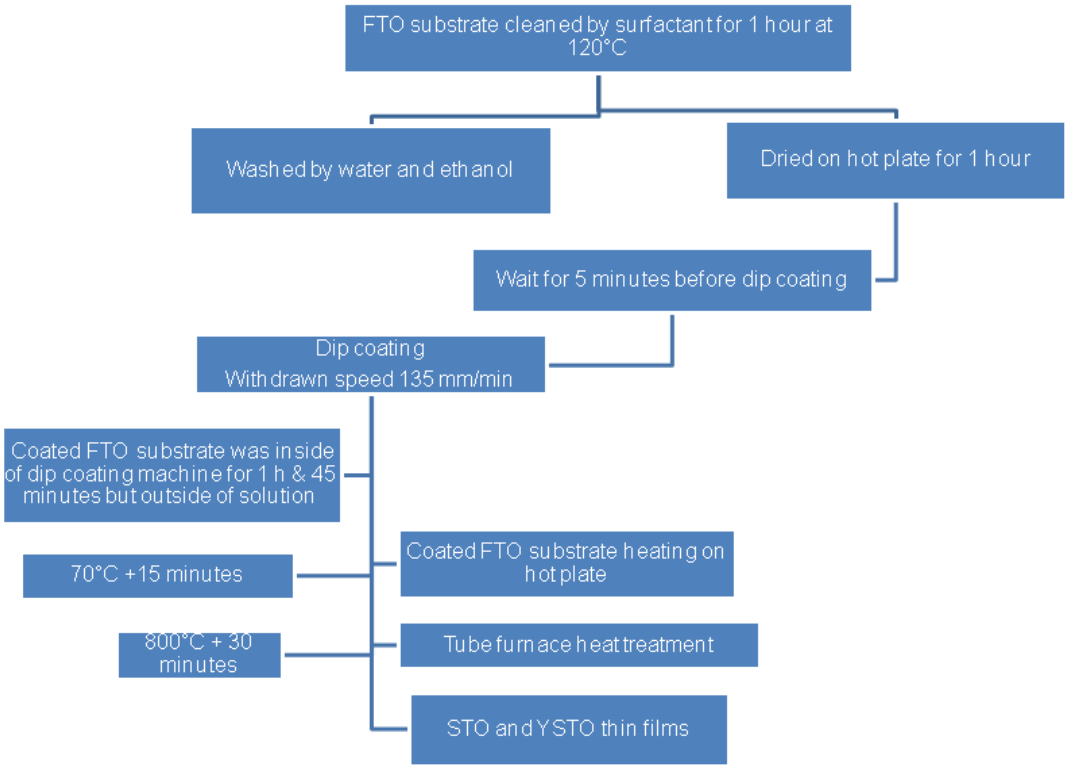

Fig 7 – Schematic procedure for film preparation.

It was found that 6 layers deposition and 4 times heat treatment produced best photocurrent in case of Y doped SrTiO3 photo-electrodes.After studying the deposition parameter for pure and Y-doped $SrTiO_3$, it was classified a better deposition condition as 6 times deposition and 4 times heat treated. In this case, it was prepared samples to study the influence of an extra heat treatment at 800°C for 30 minutes using different atmosphere (air, nitrogen and oxygen) on electrochemical/ photoelectrochemical properties. In addition, it was also prepared Ni-doped $SrTiO_3$, following the same schedule for Y-doped showed at Fig 5, with 1% mol of Ni precursor $[Ni(NO_3)_2.6H_2O]$ added just after the addition of $SrCO_3$ at the final stage. Table 4 presents the samples related to the atmosphere of extra heat treatment.

Table 4. Details of samples prepared 6 times deposition and 4 times heat treated and submitted an extra heat treatment in N_2 and O_2 gas flux.

	Deposition times (Air)	**Heat treatment times (Air)**	**Atmosphere of extra heat treatment**
STO 4 6 (N_2)	6	4	N_2
STO 4 6 (O_2)	6	4	O_2
YSTO 4 6 (N_2)	6	4	N_2
YSTO 4 6 (O_2)	6	4	O_2
NiSTO 4 6 (N_2)	6	4	N_2

3.2 Characterization

The crystallinity and phase formation was analyzed performing X-ray diffraction measurement using a diffractometer (D8 Discover, Bruker-ASX) configured with a CuKα radiation source. Film morphology was evaluated by scanning electron microscopy (SEM) carried out using FEI Inspect F50 microscopy (LIEC – UFSCAR, São Carlos, Brazil). Absorbance spectra in the ultraviolet-visible region (UV-Vis) were collected by a spectrophotometer Varian Cary 50 where bare FTO substrate was used as the blank.

Additionally, photoelectrochemical measurements were performed in a three-electrode electrochemical cell by using a potentiostat/galvanostat (μAutolab III). KCl saturated Ag/AgCl and platinum foil were used as the reference and counter electrode, respectively. The measurements were carried out in a NaOH solution (1M, pH= 13.6 at 25°C) with the prepared photoanodes acting as working electrode. It was used an AM 1.5G simulated sunlight (100mW/cm^2) using 450 xenon lamp (ozone free) for photoelectrochemical measurement. Linear sweep measurement (current density vs applied potential) was done at dark and light condition at a scan rate of 50 mv s^{-1}. Chronoamperometry (Current vs time) was done at light conditions at potential 1.23 $V_{RHE.}$ Electrochemical impedance spectroscopy (EIS) measurements were performed to measure resistivity in the thin films by using potentiostat/galvanostat (Autolab PGSTAT129N) coupled to a Faraday cage. Additionally, Mott-Schottky measurements were performed under dark condition where DC potential range

was 0.2-1.8 V_{RHE} and AC frequency was in the range from 10 kHz to 1 Hz to estimate electrochemical parameters such as donor density and impedance. The amplitude of AC potential was 10 mV. These measurements were carried out in the Laboratory of Alternative Energy and Nanomaterials (LEAN) at *Universidade Federal do ABC*.

4. RESULTS

In this section, it will be presented the most important results for preparation of pure and doped-$SrTiO_3$ photoanodes. Firstly, it has been made a discussion about deposition procedure and set the best condition achieved for pure and Y-doped STO photoanodes.

In the sequence was discussed an optimization in this procedure aim improving more the photoanode photoelectrochemical performance. It was made a study of using an additional heat treatment with different atmospheres and the influences on photoanodes properties. Finally, an incorporation of another dopant (nickel) has been discussed.

4.1 Pure and Y-doped STO photoanodes: deposition optimization

The films are thin, transparent and homogeneous (Fig 8). The outside transparent material of each film is epoxy which was used to make sure better control of the immersed electrode area.

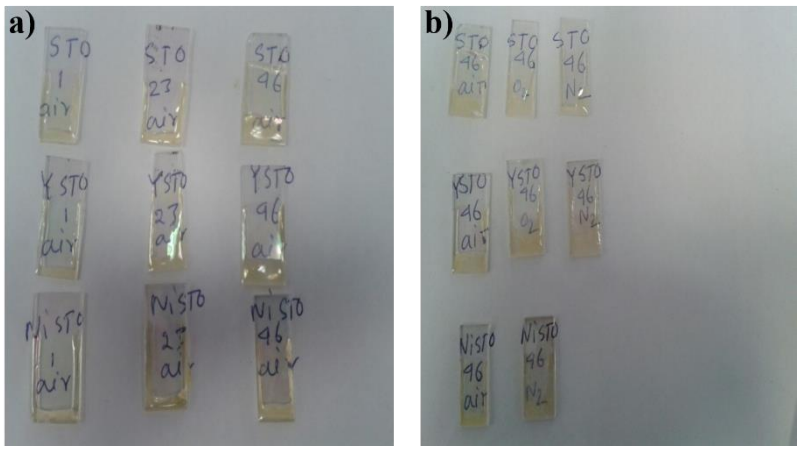

Fig 8 – Image of the prepared thin films pure and Y / Ni-doped STO. a) Films pure and doped (Y or Ni) synthesized with different depositions and heat treatment; b) STO 46 deposition condition (pure and doped) with different atmosphere conditions.

The crystalline structure of the prepared thin film was evaluated by X-ray diffraction experiment. Fig 9 illustrates the X-ray diffraction pattern with all peaks indexed as being pure

phase of strontium titanate. XRD analysis has been made only for the best deposition thin films.

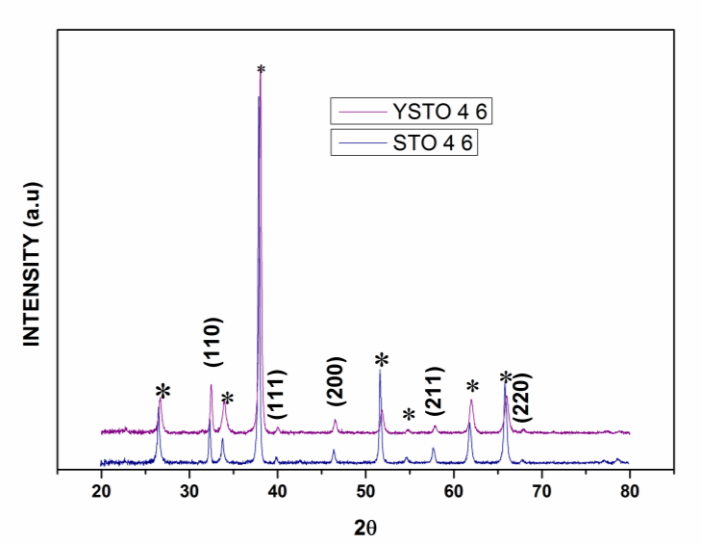

Fig 9 - XRD patterns of Strontium titanate photoanodes deposited on FTO glass substrate deposited 4 times and 6 times heat treated. The additional peaks indicated by asterick (∗) are related to casseterite phase from conductive layer of substrate ($F:SnO_2$).

From the Table 5 below, it has seen that unit cell parameter according to crystallographic file number (JCPDS 79-0176) is in accord with experimental results.

Table 5 - Lattice parameter of pure and Y-doped STO thin films.

Sample	**a(Å)**	**V(Å^3)**
JCPDS 79-0176	3.905	59.547
STO 4 6	3.896 ± 0.007	59.154 ± 0.302
YSTO 4 6	3.900 ± 0.001	59.320 ± 0.040

Results agree with the standard values from crystallographic file and confirm a presence of a cubic structure. For Y-doped photoanodes was not noticed changes, considering measurements error, on the unit cell parameter. This result avoids confirming that Y was doped inside of SrTiO3 structure. Moreover, the shift of 2θ angle observed on Fig 9 towards higher angle may be result of instrumental error.

To analyze photoanodes morphologies, it was performed scanning electronic microscopy (SEM). Fig 10 illustrates SEM top-view images for different deposition conditions.

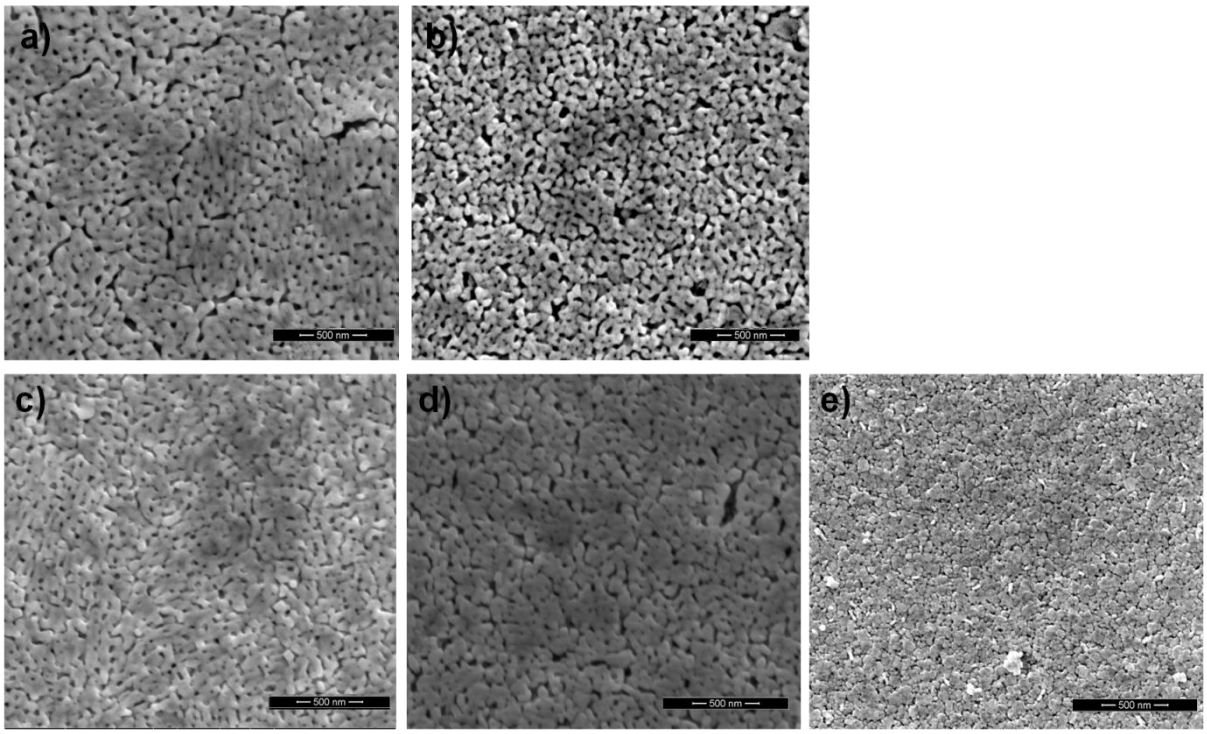

Fig 10 - TOP view SEM image of STO and YSTO photoanodes; a) STO 1, b) STO 2 3 c) YSTO 1, d) YSTO 2 3, e) YSTO 4 6.

It has been indicated from the SEM image for STO 1 and YSTO 1 that these two had similar smooth surface and uniform distribution of worm-like grains. The average length of the worm-like grain was calculated by *Image J* software where were found values: STO 1 (128.541 nm), YSTO 1 (121.665nm), STO 2 3 (127.627 nm), YSTO 2 3 (97,860 nm), YSTO 4 6 (82.229 nm). It has been seen from results that length has been decreased increasing deposition and heat treatment times. It can also be confirmed that these worm-like morphologies have been thicker with the increase in thickness. Moreover, it has also been found some cubic structure in case of YSTO 4 6 thin films.

Then, to find out if the prepared thin films will absorb UV-visible light range it was performed the UV-Visible spectroscopy as illustrated in the Fig. 11 below.

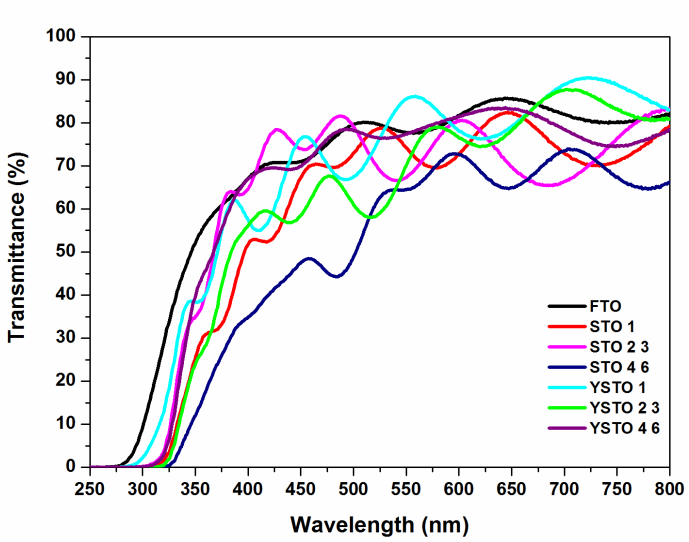

Fig 11 - UV-visible spectroscopy showing the change in transmittance spectra depending on the layers of each STO and YSTO photoanodes.

From UV- Visible spectroscopy, it is possible to see that absorbance has been increased with the increase in deposition layers. As the deposition times increases the film thickness an increase in absorption coefficient is expected. Later, it was investigated the photoelectrochemical performance of pure and Y-doped STO photoanode synthesized with different deposition procedures. It was carried out the photoelectrochemical measurement in presence and absence of light. The photocurrent response is showed in Fig 12.

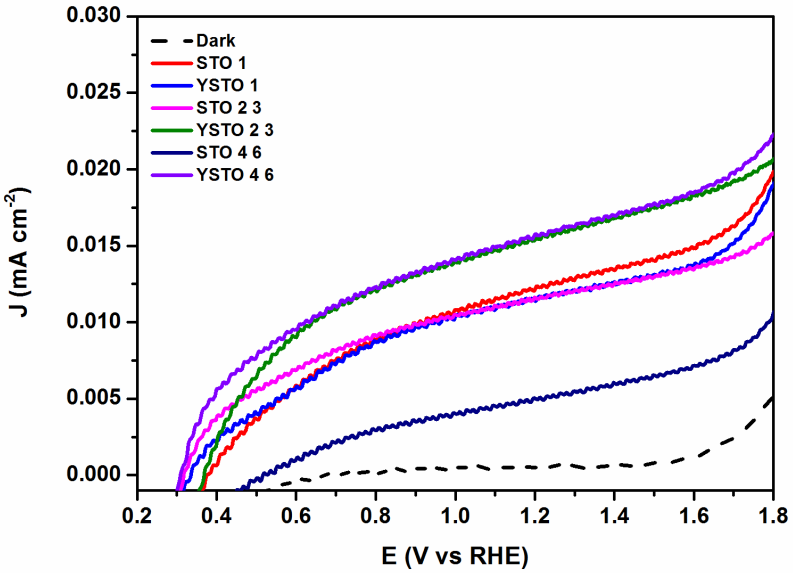

Fig 12 - Linear sweep voltammetry graph of STO and YSTO samples under front side illumination.

The photoelectrochemical performances of produced STO and Y-doped STO photoanodes were evaluated by linear sweep voltammetry (J vs V_{RHE}) in the dark and sunlight simulated condition. All photo anodes showed lowest currents in the dark .

After illumination, all photoanodes showed reasonable photocurrent at 1.23 V_{RHE}. From Table 6, it was found that the STO 1 and YSTO 1 thin films have exhibited the same photocurrent values that could be related to their similar morphology. For STO 2 3 and YSTO 2 3 photoanode, the Y-doped had highest photocurrent density because its surface is highly porous that means a large surface area. In case of STO 4 6 and YSTO 4 6, YSTO 4 6 had the highest photocurrent because it is highly crystalline with preferred cubic crystal structure. Hence from table 6, it is possible to see that Y-doped STO showed highest photocurrent than undoped STO photoanode and photocurrent value increases with deposition and heat treatment times. But, photocurrent values for pure STO photoanodes decreases with the increase in deposition and heat treatment times.

Table 6 - Showing the current density values of each STO and Y-doped STO thin films.

SAMPLE	**PHOTOCURRENT DENSITY (mA cm^{-2}) at 1.23 V_{RHE}**
STO 1	0.012
YSTO 1	0.012
STO 2 3	0.012
YSTO 2 3	0.016
STO 4 6	0.005
YSTO 4 6	0.016

Additionally, in order to analyze photocurrent stability in the water oxidation potential (1.23V_{RHE}), it was realized chronoamperometry measurement (Fig 13).

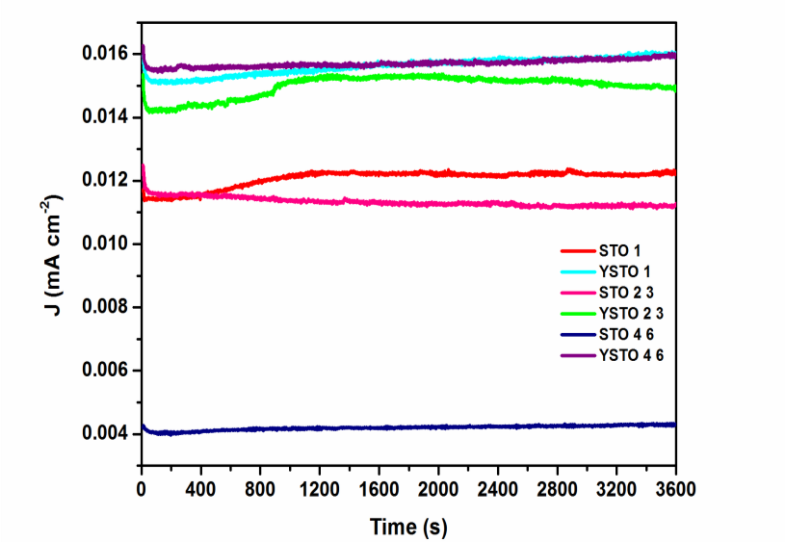

Fig 13 – Chronoamperometry showing the stability of each STO and YSTO samples under front side illumination.

Chronoamperometry measurement was done for 1 hour duration at 1.23 V $_{RHE}$ simulated sunlight condition. All samples showed decrease in stability in first few seconds and then it was quite stable. In order to investigate the stability and material release to the solution, it was performed cyclic voltammetry experiment (Fig 14) for undoped and doped films.

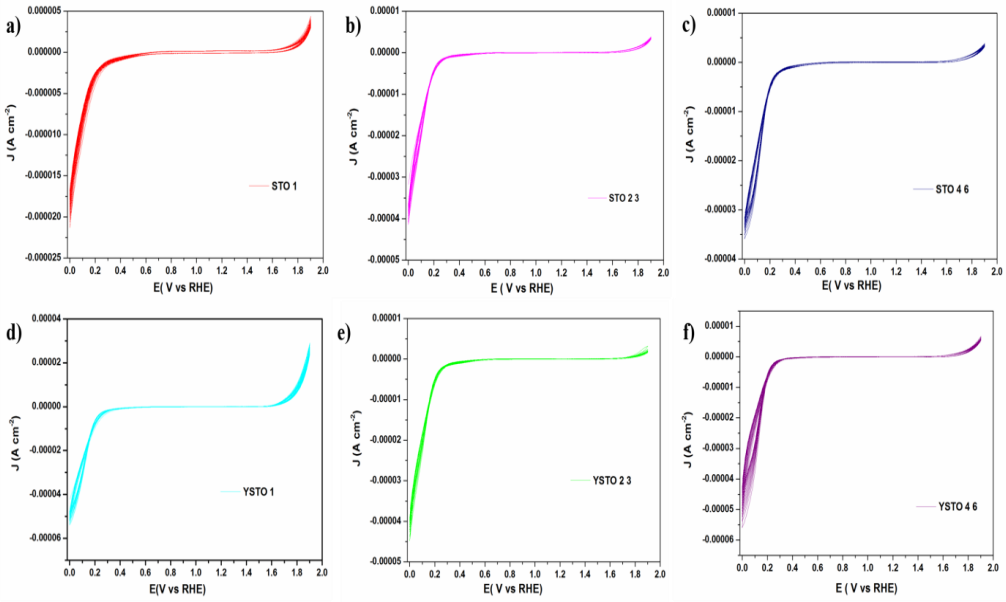

Fig 14 - Cyclic voltammetry measurement graph for STO and YSTO: a) STO 1, b) STO 2 3, c) STO 4 6, d) YSTO 1, e) YSTO 2 3, f) YSTO 4 6.

The cyclic voltammetry experiments were performed for 20 cycles. From this measurement, it was possible to notice that there is no species released from the STO and YSTO photoanode to solution, which confirm that the STO and YSTO photoanode are stable in electrochemical solution. To analyze the electronic properties of the interface electrode-electrolyte the electrochemical impedance spectroscopy (EIS) was performed. Fig 15 shows resistance for charge transfer by Nyquist plots for doped and undoped STO photoanodes.

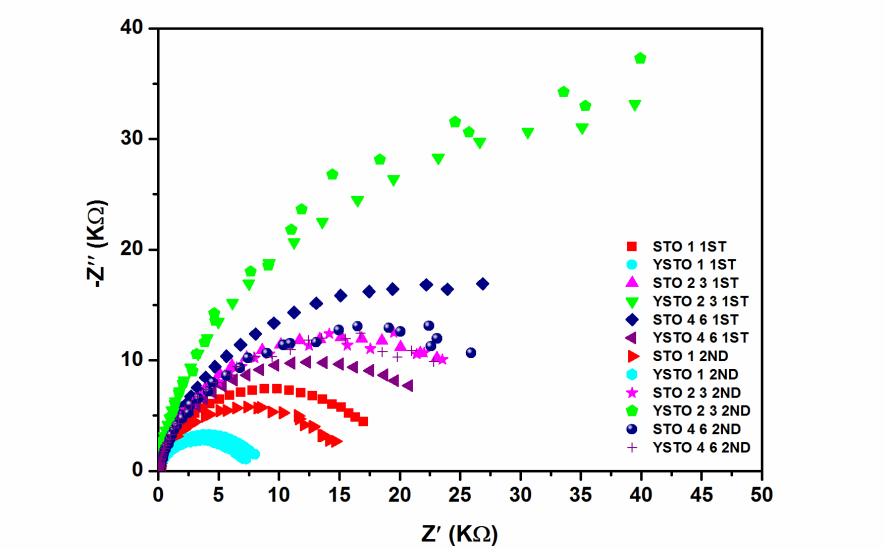

Fig 15 – Electrochemical Impedance Spectroscopy measurement for STO and YSTO photoanodes synthesized in different deposition and heat treatment times.

From EIS data it was observed that the YSTO 1 has lowest resistivity (it can be hypothesized that YSTO 1 thin film might have less defects) whereas the YSTO 2 3 exhibited highest resistivity to charge transfer(possible hypothesis for this sample is that YSTO 2 3 thin films might have more defects). In order to estimate the donor density value, it was used the Mott-Schottky analysis. The Fig 16 shows the linear adjust of the Mott-Schottky plots for different photoanodes.

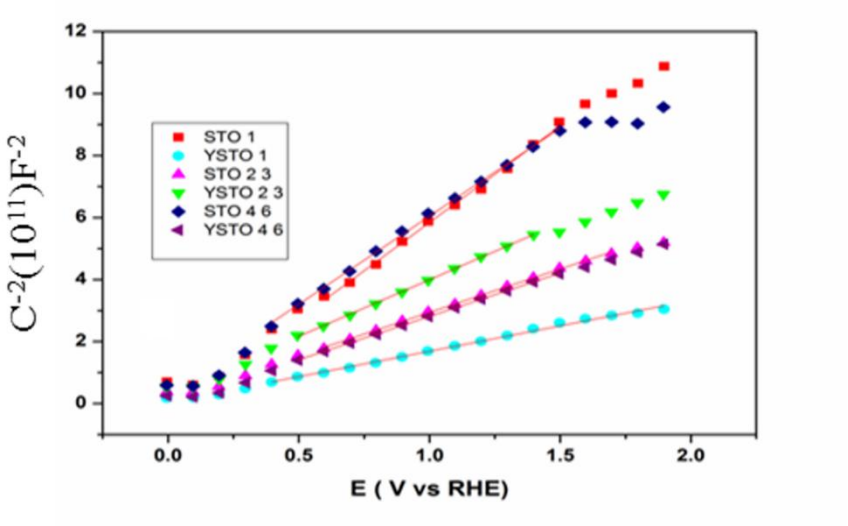

Fig 16 - Mott- Schottky plot for all photoanodes synthesized. For this measurement, the same a three-configuration cell and electrolyte was used. The linear adjust was done at frequency of 10 KHz.

From Mott-Schottky the donor density was calculated by using the following equation:

$$N_D(cm^3) = \frac{1.41x10^{32}}{\varepsilon_r A^2 slope} \quad (5),$$

where 1.41 x 10^{32} (cm F^{-2} V^{-1}), ε_r is permittivity equal to 200 for $SrTiO_3$ [25], A^2 (cm^4) is the emerged photoelectrode area and the slope (F^{-2} V^{-1}) is from linear adjustment of Mott-Schottky plot. The calculated values of donor density values were summarized in the Table 7.

Table 7 – The estimated donor density values from Mott-Schottky data.

SAMPLE	**N_D(cm^{-3})**
STO 1	1.97 X 10^{19}
YSTO 1	3.51 X 10^{19}
STO 2 3	1.57 X 10^{19}
YSTO 2 3	4.82 X 10^{19}
STO 4 6	1.58 X 10^{19}
YSTO 4 6	2.46 X 10^{19}

The photocurrent density was almost similar in magnitude for all samples because the donor density was almost similar in magnitude for all samples.

4.2 $SrTiO_3$ best synthesis condition

After systematic study and all the characterizations of STO and Y-doped STO related to deposition, it was noticed that the best photoelectrochemical response achieved for this material was presented by STO 4 6. So, it was set to study strontium titanate photoanodes prepared by 6 times deposition and 4 times heat treatment. Thus, this section is dedicated to a detailed study of the samples synthesized in this condition.

Additionally, it was varied parameters such as: heat treatment atmosphere and insertion of dopants (yttrium and nickel). All the samples were analyzed by optical, structural, morphological, electrochemical and photoelectrochemical properties to achieve a better material performance to be applied as photoanode in a photoelectrochemical cell.

4.2.1 Optical, structural and morphological properties for pure and doped STO 4 6 thin films heat treated at different atmospheres

Diffractograms present in Figure 17 for different samples pure and doped with distinct atmospheres. The peaks were indexed in a cubic phase for $SrTiO_3$ using a standard crystallographic file (JCPDS 79-0176). It was not found peaks referring to other materials or structures and the extra peaks indicated by asteric (∗) found related to the cassiterite phase of tin oxide (SnO_2) from conductive layer on the substrate (FTO / F: SnO_2).

In addition, preferential orientation was calculated for all photoanodes using Lotgering´s equation [47, 48, 49] which were presented on Table 8. It was noticed that all films have presented a preferential plane through to the (110) plane. This is an important result once this plane was related to improvement of the films conductivity. This plane is perpendicular to the basal plane and perpendicular to the substrate which means more efficient charge transfer through depletion layer. Consequently, strontium titanate containing preferential orientation (110) has been applied in photoelectrochemical devices for better charge transfer process through depletion layer.[50]

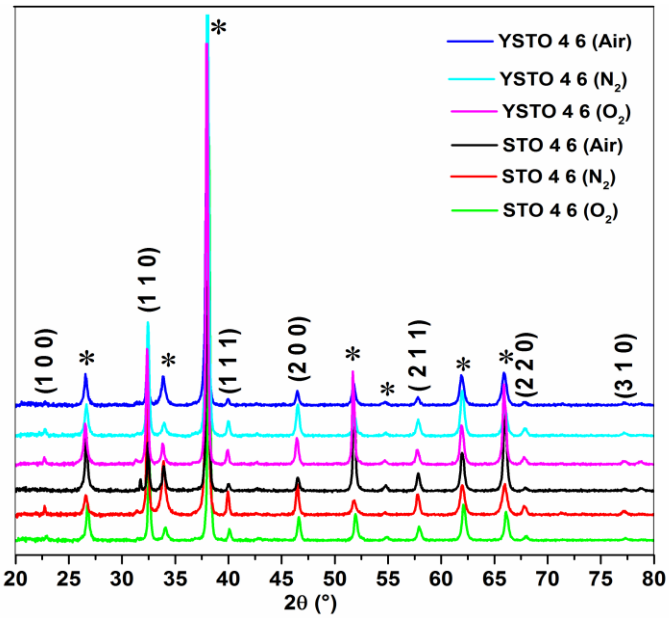

Figure 17. X-ray diffraction study of pure and Y doped STO 4 6 thin films on FTO substrate. Asterisks (∗) indicate peaks associated with F: SnO_2 on glass substrate.

Through the XRD patterns, it was possible to estimate the unit cell parameters and cell volume using free software (*Cellcalc*). The calculated values were compared with those values found in the standard diffraction card (JCPDS – 79-0176) and summarized at Table 8. Additionally, it was determinate the crystallite size for preferential orientation plane (110) by using Scherer equation.[51]

Table 8 – Lattice parameter (*a*) and cell volume (*V*) calculated from XRD patterns for STO pure and Yttrium-doped in different atmospheres compared to a crystallographic standard card for cubic structure. In addition, it is showed the preferential orientation (P.O.) and crystallite size for all samples.

Sample	*a* (Å)	*V* (Å^3)	P. O.	Crystallite size (nm)
JCPDS 79-0176	3.905	59.547	-	-
STO 4 6 (Air)	3.900 ± 0.001	59.328 ± 0.033	(110)	38
STO 4 6 (O_2)	3.8906 ± 0.001	59.130 ± 0.055	(110)	37
STO 4 6 (N_2)	3.902 ± 0.001	59.407 ± 0.036	(110)	33
YSTO 4 6 (Air)	3.909 ± 0.003	59.752 ± 0.126	(110)	35
YSTO 4 6 (O_2)	3.906 ± 0.001	59.608 ± 0.031	(110)	31
YSTO 4 6 (N_2)	3.903 ± 0.001	59.472 ± 0.026	(110)	38

The lattice parameter values (unit cell edge length (a) and unit cell volume (V)) obtained for STO 4 6 prepared at air, nitrogen and oxygen atmosphere are in good agreement with the values reported in literature for undoped $SrTiO_3$. [25, 52] After doping, lattice parameter values did not increase very much as we expected. The crystallite size values for undoped strontium titanate photoanodes are also in agreement with the literature values.[52] The size of Y^{3+} is 0.90 Å and crystal structure is HCP, in other hand, the size of Sr^{2+} is 1.18 Å and crystal structural is FCC.[53] Due to difference in crystal structure, valence, size and electronegativity of Sr^{2+} and Y^{3+}, probably, Y^{3+} could not replace Sr^{2+}, as a result, lattice parameter and crystallite size values were similar in pure and Y-doped $SrTiO_3$.

In order to investigate the optical properties of STO 4 6 films (doped and undoped) heat treated at different atmosphere, it was analyzed transmittance spectra by using a spectrophotometer at UV-visible range. Figure 18 shows the spectra for all samples treated at different atmosphere.

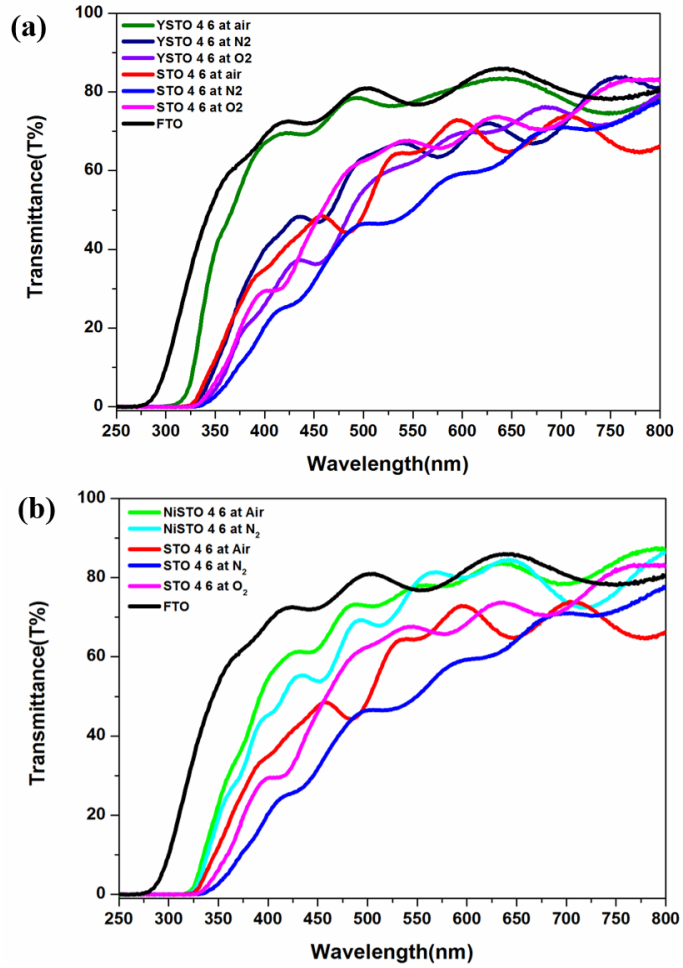

Fig 18- UV – Visible spectroscoy of (a) STO 4 6 and YSTO 4 6 at air , O_2 , N_2; (b) STO 4 6 at air, O_2, N_2 and NiSTO 4 6 at air, N_2 atmosphere. Undoped STO 4 6 samples added in both graphs for better comparison.

The maximum absorption of blank substrate (FTO substrate) was around 270 nm. The pure STO 4 6 photoanodes prepared at 800ºC in air condition shows a maximum absorption around 325 (nm). Pure STO 4 6 photoanodes subbmited at N_2 or O_2 atmosphere were prepared by using the same procedure as the pure one at air condition. In Figure 18a, it was observed that YSTO 4 6 at air , N_2 and O_2 showed absorption maximum value between 320-345 nm. The same profile was observed for Ni-doped (Fig18b) with maximum around 325 and 330 at air and N_2, respectively.

The photoanodes extra heat treated at N_2 and O_2 atmosphere had higher absorption towards visible spectrum than those treated in air condition. It could be explained by band gap engineering phenomena. For example, with the introduction of dopant like Y, it is possible to create mid band gap levels which increases absorption towards visible

spectrum.[45] Then, another kind of doping is introducing oxygen vacancy. For instance, yttrium can be incorporated into $SrTiO_3$ by following way[58]:

$$Y_2O_3 \xrightarrow{SrTiO3} 2Y^{\bullet}_{Sr} + V''_{Sr} + 3O_O$$

By balancing charge mass and site, the above equation can be written as follows:

$$SrO + Y_2O_3 + 4\ TiO_2 = 2Y^{\bullet}_{Sr} + V''_{Sr} + Sr_{Sr} + 4\ Ti_{Ti} + 12O_O$$

Uppon reduction of Y doped $SrTiO_3$, oxygen vacancies and electrons are generated by using the following equation:

$$O_O = \frac{1}{2}O_2(g) + V^{\bullet\bullet}_O + 2e^-$$

Electron transport described by large polaron model is generally associated with titanium ions as follows:

$$Ti^{4+} + e^- = Ti^{3+}$$

By combining the immediate above two equation, reduction reaction in Y doped $SrTiO_3$ and creation of oxygen vacancies can be written as follows :

$$2Ti_{Ti} + O_O \xrightarrow{SrTiO3} 2Ti'_{Ti} + V^{\bullet\bullet}_O + \frac{1}{2}O_2(g)$$

where, $Y^{\bullet}_{Sr}$ means yttrium with one positive charge with strontium substitution, V''_{Sr} means Sr vacancy with doubly negative charge, O_O means oxygen atom in its lattice site, Sr_{Sr} means Strontium atom in its lattice site, Ti_{Ti} means Ti atom in its lattice site, $V^{\bullet\bullet}_O$ means oxygen vacancy with doubly positive charge, Ti'_{Ti} means Ti in its lattice site with one negative chagre.

This oxygen vacancies could be created when $SrTiO_3$ thin film is treated at temperature above 600ºC.[46] As these films were treated at 800ºC, there is a great possibility to produce oxygen vacancy which is also another reason for absortption moving towards visible spectrum. In addition , oxygen vacancies can be fullfiled at fabrication process which was done at N_2 flux.

4.2.2 Electro/Photoelectrochemical performances

Photoelectrochemical measurements were annalyzed by linear sweep voltametry in a dark and light conditions. This experiment was done in presence of sunlight simulator coupled with an AM 1.5 G filter and adjusted at 100 mW/cm^2.

Hydrogen and oxygen evolution reaction can be explained by looking at the current density value from linear sweep voltametry. After creating electron–hole pairs on our working electrode ($SrTiO_3$) , electron moves from working electrode towards counter electrode with the help of external circuit. Once this electrons reaches the metalic counter eletrode a chemical reaction take a place generating hydrogen, whereas on the semiconductor side (working electrode) an oxidative reaction occurs due presence of positive charge (h^+, hole) releasing oxygen gas. All eletrochemical and photeletrochemical experiments were conducted using 1 mol NaOH aqueous solution as a electrolyte at adjusted pH 13.6.

Fig 19 shows photocurrent density profile in function of applied potential in a alkaline medium for pure and doped STO 4 6 films heat trated at different atmosphere conditions.

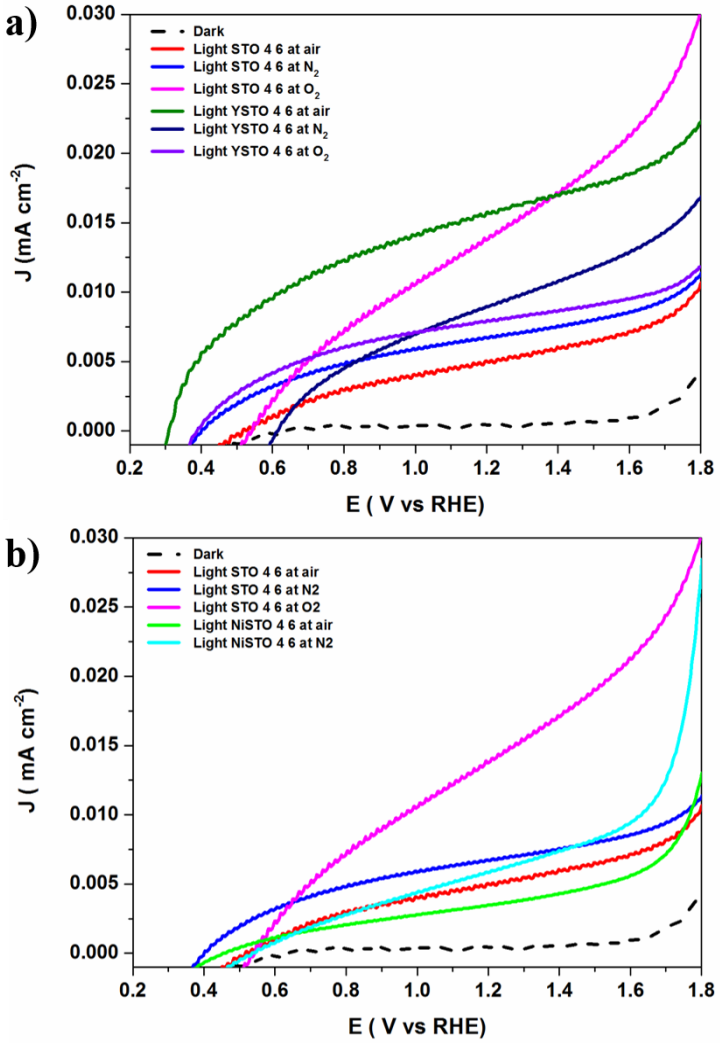

Fig 19 - a) linear sweep voltametry of STO 4 6 and YSTO 4 6 prepared all in air , O_2 and N_2 atmosphere. b) linear sweep voltametry of STO 4 6 and YSTO air , O_2 and N_2 and NiSTO 4 6 at air , N_2 atmosphere .

In the Figure 19a-b have noticed that in an absence of light it was not observed catalytic response for all photoanodes.it was measured photocurrent at dark to compare photocurrent generated in light. However, in a presence of light it has been seen an increase in solar water splitting efficieny, which means there was an efficient electron-hole pair separation which was responsible to improve photo-catalytic performances. In this work, maximum value of photocurrent was achieved for STO 4 6 submmited to N_2 atmospehere with value of 0.006 mA cm^{-2} followed by STO 4 6 at air (0.005 mA cm^{-2}). In this experiment, it was possible to notice a shift of onset potential towards more positive potential which clearly indicates the catalytic activity of the different atmospheric condition.

Freitas and co-workers [50] have reported using O_2 and N_2 atmosphere in case of photoelectrochemical water splitting for hematite photoanodes. It was discussed that the increase on the photoelectrochemical response for photoanodes heat tretaed at N_2 atmosphere is due to an improvement on solid-solid interface faciliting charge colect and transport. The authours elucidated, as well, N_2 atmosphere can act positevely on photoanode surface improving catalytic efficiency.

Interestingly , in this work highest photocurrent was found as 0.014 mA cm^{-2} for STO4 6 heat treated at O_2 atmosphere. This photocurrent improvement might be the result of the improvement of solid-liquid interface due to the extra heat treatment at O_2 atmosphere as reported on literature.[50] The another explanation is The shift towards more anodic potential in case of STO 4 6 at O_2 can positively affecting band bending which results in better charge separation process. This result permits to conclude that the extra heat treatment at oxygen atmosphere enhace charge transport and decrease charge recombination.

In the case of Y-doping photoanodes, it was achieved a photocurrent of 0.016 mA cm^{-2} for YSTO 4 6 films at air. After submmiting to an extra heat treatment at N2 and O2 atmosphere, it was observed that YSTO 4 6 at N_2 has presented more shift towards anodic potential than YSTO 4 6 at O_2. YSTO 4 6 at N_2 has shown a slight improvement on photocurrent with value of 0.010 mA cm^{-2}. On the other hand, YSTO 4 6 at O_2 gave photocurrent value 0.007 mA cm^{-2}. For Y-doped photoanodes an additional heat treatment in different atmospheres did not show good results compraing with that heat treated in air condition.

Additionally, for NiSTO 4 6, photocurrents were too small where the photocurrent values of NiSTO 4 6 at air and N_2 was 0.003 mA cm^{-2} and 0.006 mA cm^{-2} . The photocurrent decrease is due to competitive light absorption by Ni particles(if Ni could not replace Ti) in

the UV spectrum range which increases electron hole recombination at the Ni–STO site and Ni particles acts as electron trapping.[54]

Fig 20 illustrates photocurrent stability for STO photoanodes pure and doped with different atmospheres.

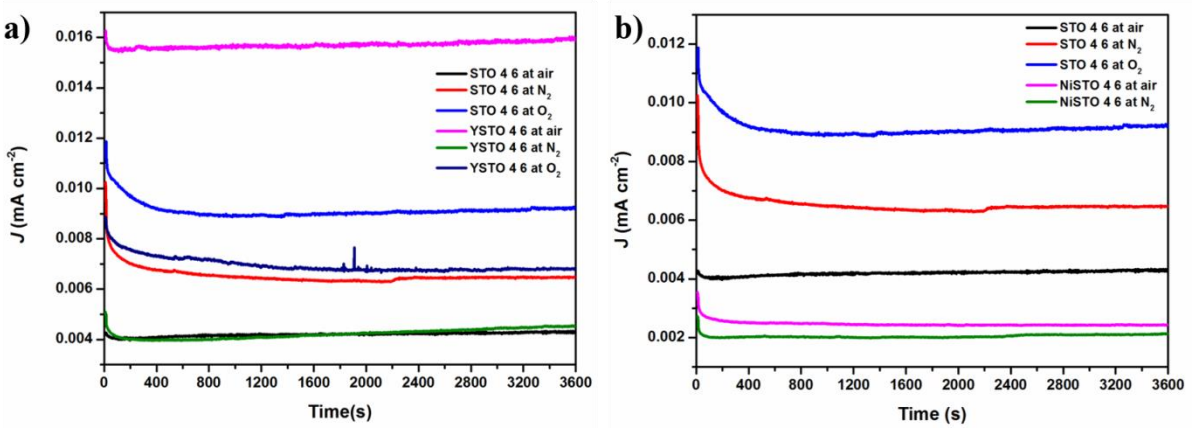

Fig 20 - Chronoamperometry study of (a) STO 4 6 and YSTO 4 6 at air, N_2, O_2 atmosphere; (b) STO 4 6 at air, O_2 , N_2 and NiSTO 4 6 at air , N_2 atmosphere .

The main purpose of 1 hour duration chronoamperometry was to evaluate photocurrent stability at water oxidation potential. It has found that these photoanodes stability decrease in the first minute and then all quite stable until experiments end. This result is very good to apply these photoanodes to use industrially.To use these photo-electrodes industrially, it must have to be stable for longer period of time without decreasing current density. The films STO 4 6 and YSTO 4 6 at air are more stable than films prepared at N_2 and O_2 atmosphere. In addition, it was observed a little increase in photocurrent density at the end of each experiment, it could be related to wettability improving surface area in contact with the electrolyte.

The resistance for charge transfer was analyzed by EIS using Nyquist plots. Fig 21a shows a comparison between pure and Y-doped photoanodes heat treated in air and those submitted an extra heat treatment at nitrogen and oxygen atmosphere. In addition, Fig 21b presents the comparison between pure and Ni-doped photoanodes in different conditions of atmosphere as well.

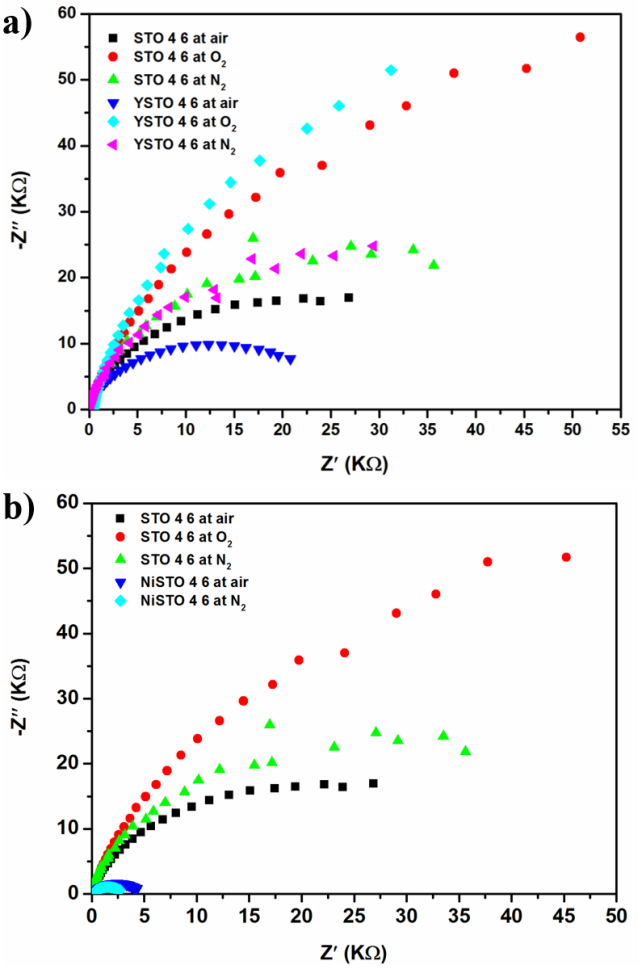

Fig 21 – Eletrochemical Impedance spectroscopy analysis of STO 4 6, NiSTO and YSTO 4 6 prepared at air, O_2, N_2 atmosphere. (a) STO 4 6 and YSTO 4 6; (b) STO 4 6 at air, N_2, O_2 and NiSTO 4 6 air, N_2 atmosphere. In both plot the STO was included for better comparison.

By Nyquist plots, It was noticed that resistance to charge transfer for STO 4 6 and YSTO 4 6 with additional heat treatment at O_2 and N_2 atmosphere has been increased. This fact can be explained by polaronic nature of $SrTiO_3$. The valence number of Titanium ion can be alternated into +3 and + 4 within a time scale greater than 1 $x10^{-16}$ s. Electrons inside of $SrTiO_3$ are in polarization field which is produced with the displacements of Ti^{4+} and O^{2-} in TiO_6 octahedron. So, the conduction electrons with polarization field are called polaron. When SrTiO3 photoanode is heated in O_2 flux, polaron size of $SrTiO_3$ is changed due to the adsorption of O_2. The larger the size of polaron is the higher material conductivity. [55,56] Consequently, it could explain the lower conductivity in case of O_2 heat treated photoanodes.

In addition, in case of electron doped (Y) $SrTiO_3$, polaron size of SrTiO3 decreases. The ionicity of $SrTiO_3$ increases with the adsorption of eletronegatively oxygen on the SrTiO3 surface rising up resistivity. Morever, when O_2 is adsorbed on the $SrTiO_3$ (pure and

Y-doped) photoanodes distorts TiO_6 unit cell which traps the conduction electrons to flow.[46,55] In case of nitrogen atmosphere, because of the presence of less oxygen partial pressure, there is a production of oxygen vacancy that could improve conductivity and explain lower resistivity for charge transfer.

In order to analyze donor density, it was made a linear adjust from Mott-Schottky graphs. Fig 22 shows the curves and the adjustment.

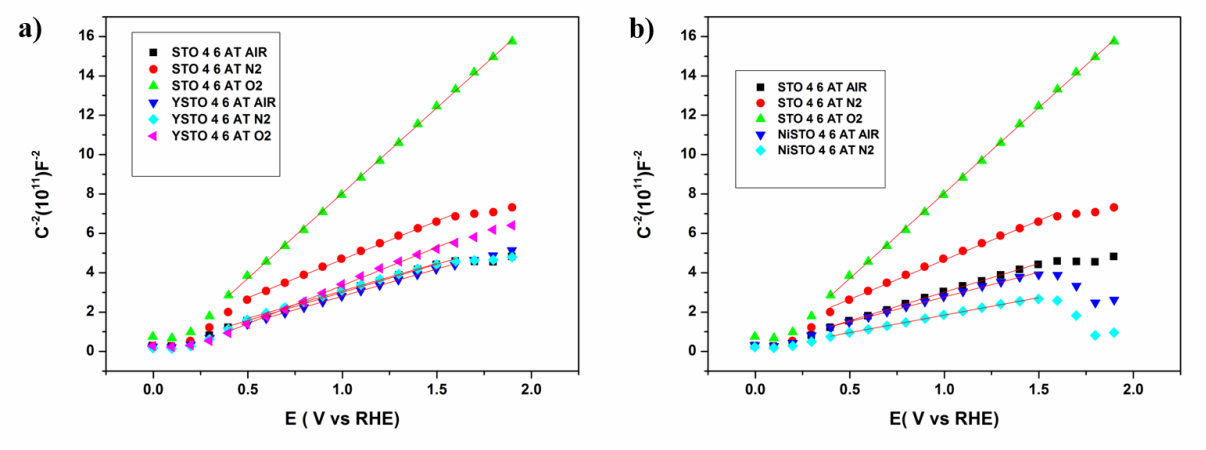

Fig 22 - (a) Mott-Schottky analysis of STO 4 6 and YSTO 4 6 at air,O_2, N_2 atmosphere; (b) Mott-Schottky analysis of STO 4 6 at air, N_2, O_2 and NiSTO 4 6 at air, N_2 atmosphere.

Linear adjustment from Mott-Schottky curves was analyzed to determine photoanodes donor density by using Equation 2. Fig 21a presents curves related to pure and Y-doped photoanodes with different atmosphere conditions. In another side, Fig 21b shows curves referring to pure and Ni-doped photoanodes also with different atmosphere conditions. Calculated values are summarized in Table 9 for all photoanodes.

Table 9 - Calculated donor density (N_D) of STO 4 6, YSTO 4 6 and NiSTO 4 6 with different atmospheres (air, O_2 and N_2).

	N_D (cm^{-3})
STO 4 6 (Air)	$3.08\ 10^{19}$
STO 4 6 (N_2)	$4.40\ 10^{19}$
STO 4 6 (O_2)	$4.81\ 10^{19}$
YSTO 4 6 (Air)	$2.49\ 10^{19}$
YSTO 4 6 (N_2)	$2.05\ 10^{19}$
YSTO 4 6 (O_2)	$2.31\ 10^{19}$
NiSTO 4 6 (air)	$1.32\ 10^{19}$
NiSTO 4 6 (N_2)	$3.05\ 10^{19}$

Photoanodes with additional heat treatment at O_2 and N_2 atmosphere has shown a slight increase on donor density considering similar order of magnitude. It was found that STO 4 6 at O_2 has higher donor density which could explain a higher photocurrent than films STO 4 6 at N_2 and air, even in a small difference. On other hand, for Y-doped $SrTiO_3$ donor density was not increased very much as it was expected. In case of NiSTO 4 6 photoanodes, donor density has increased with an extra heat treatment at nitrogen atmosphere. However, It can be understood that donor density of of undoped samples are higher than the denor density of doped samples. It can be hypothesized that Y and Ni dopant might not their their host element Sr and Ti respectively. As a result, donor density was lower for doped samples than undoped samples.

5. CONCLUSION

In UV-visible spectroscopy, it was found some additional peaks in the visible range which corresponds to the presence of oxygen vacancies due to heat treatment above 600ºC or additional heat treatment at O_2 and N_2 atmosphere. The additional peaks could also be related to the presence of mid band gap level due to the insertion of dopant like yttrium and nickel.

In the case of photoelectrochemical response of pure STO 4 6 submitted to oxygen atmosphere was highest in case of pure strontium titanate. So, it was concluding that oxygen atmosphere could improve solid–liquid interface positively which favors high catalytic response.

After introducing yttrium, the highest photocurrent response was observed for YSTO 4 6 at air. However, there was a clear catalytic response, thus onset potential shifted towards more anodic potential with extra heat treatment at N_2 and O_2 atmosphere. The same was true for NiSTO 4 6 photoanodes which were only prepared at air and N_2 atmosphere with higher photocurrent response for NiSTO 4 6 at N_2.

Finally, it was a deal working with deposition steps in this work and was determinate that increasing layers is possible to improve photoelectrochemical performance for strontium titanate photoanodes. Moreover, it has seen that an additional heat treatment using different atmospheres could be a good strategy, but combining effects (dopants + atmosphere) not always represents an improvement on photoelectrochemical performance.

6. REFERENCES

[1] Zhebo Chen, Huyen Dinh, Eric Miller. Photoelectrochemical Water Splitting Standards, Experimental Methods, and Protocols, **Springer-Verlag New York**. Available: < http://dx.doi.org/10.1007/978-1-4614-8298-7 .

[2] http://ocean.nationalgeographic.com/ocean/critical-issues-sea-level-rise/ access date – 05/05/2016.

[3] Lewis N.S, Nocera D.G. Powering the planet: chemical challenges in solar energy utilization. **Proceeding of National Academy of Sciences of United States of America**. 103, 15729–15735 (2006). Available: < http://dx.doi.org/10.1073/pnas.0603395103 >

[4] Lewis, N.S., Crabtree, G.: Basic Research Needs for Solar Energy Utilization: report of the Basic Energy Sciences Workshop on Solar Energy Utilization,April 18-21, 2005. US Department of Energy, Available: < http://www.sc.doe.gov/bes/reports/files/SEU_rpt.pdf >. Access date: 16/01/2017.

[5] Rajeshwar, K., McConnell, R., Licht, S.: Solar Hydrogen Generation – Toward a Renewable Energy Future. **Springer,** New York (2008). Available: < HTTP://dx.doi.org/10.1007/978-0-387-72810-0 >

[6] Gabriele Zini , Paolo Tartarini Solar Hydrogen Energy Systems. Springer-Verlag Mailandm. 2012, Available: http://dx.doi.org/10.1007/978-88-470-1998-0

[7] Klaus Jäger Olindo Isabella Arno H.M. Smets René A.C.M.M. van Swaaij Miro Zeman .Solar Energy Fundamentals, Technology, and Systems. **Delft University of Technology**, 2014. Access date : 16/01/2017.

[8] https://depts.washington.edu/spirolab/researchpro.html Access date - 05/05/2016.

[9] CARVALHO JR., W. M.; SOUZA, F. L. Doping effect in semiconductor nanostructure and its impact on photocatalytic performance. **Doctoral thesis.** Centro de Ciências Naturais e Humanas (CCNH), Universidade Federal do ABC, Santo André, SP, Brazil.

[10] LENG, W. H. et al. Investigation of the kinetics of a TiO2 photo-electro-catalytic reaction involving charge transfer and recombination through surface states by

electrochemical impedance spectroscopy. **The Journal of Physical Chemistry B,** v. 109, n. 31, p. 15008-23, 2005. Available: < http://dx.doi.org/10.1021/jp051821z >

[11] COWAN, A. J. et al. Water Splitting by Nanocrystalline TiO2 in a Complete Photoelectrochemical Cell Exhibits Efficiencies Limited by Charge Recombination.**The Journal of Physical Chemistry C,** v. 114, n. 9, p. 4208-4214, 2010. Available: < http://dx.doi.org/10.1021/jp909993w >

[12] LIN, Y. et al. TiO2/TiSi2 heterostructures for high-efficiency photoelectrochemical H2O splitting. **Journal of American Chemical Society.** v. 131, n. 8, p. 2772-3, 2009. Available: < http://dx.doi.org/10.1021/ja808426h >

[13] KAVAN, L.; KRATOCHVILOVA, K.; GRÄTZEL, M. Study of Nanocrystalline TiO2 (Anatase) Electrode in the Accumulation Regime. **Journal of Electroanalytical Chemistry,** v. 394, n. 1-2, p. 93-102, 1995. Available < http://dx.doi.org/10.1016/0022-0728(95)03976-N >

[14] SRINIVASAN, A.; MIYAUCHI, M. Chemically Stable WO3 Based Thin-Film for Visible-Light Induced Oxidation and Superhydrophilicity. **The Journal of Physical Chemistry C,** v. 116, p. 15421-15426, 2012. Available: < http://dx.doi.org/10.1021/jp303472p >

[15] WANG, H.; DEUTSCH, T.; TURNER, J. A. Direct Water Splitting under Visible Light with Nanostructured Hematite and WO3 Photoanodes and a GaInP2 Photocathode. **Journal of The Electrochemical Society,** v. 155, n. 5, p. F91-F96, 2008. Available: < http://dx.doi.org/10.1149/1.2888477 >

[16] GONÇALVES, R. H.; LEITE, L. D. T.; LEITE, E. R. Colloidal WO3 nanowires as a versatile route to prepare a photoanode for solar water splitting. **ChemSusChem,** v. 5, n. 12, p. 2341-7, 2012. Available: < http://dx.doi.org/10.1002/cssc.201200484 >

[17] GONÇALVES, A. D. S.; DAVOLOS, M. R.; NOGUEIRA, A. F. Efficient Dye-Sensitized Solar Cells Based on the Combination of ZnO Nanorods and Microflowers. **Journal of nanoscience and nanotechnology,** v. 10, n. 10, p. 6432-6438, 2010. Available: < https://dx.doi.org/10.1166/jnn.2010.2542 >

[18] LIN, Y.-G. et al. Microwave-activated CuO nanotip/ZnO nanorod nanoarchitectures for efficient hydrogen production. **Journal of Materials Chemistry. 21**, 324-326.2011. Available: < http://dx.doi.org/10.1039/C0JM03022H >

[19] VAYSSIERES, L. et al. Controlled aqueous chemical growth of oriented three-dimensional crystalline nanorod arrays: Application to iron(III) oxides. **Chemistry of Materials,** v. 13, n. 2, p. 233-235, 2001. Available: < http://dx.doi.org/10.1021/cm001202x >

[20] INGLER, W. B.; BALTRUS, J. P.; KHAN, S. U. M. Photo-response of p-type zinc-doped iron (III) oxide thin films. **Journal of American Chemical Society,** 126(33):10238-9, 25 Aug 2004, Available : < http://dx.doi.org/10.1021/ja048461y >

[21] KLEIMAN-SHWARSCTEIN, A. et al. Electrodeposition of α-Fe2O3 Doped with Mo or Cr as Photoanodes for Photocatalytic Water Splitting. **Journal of Physical Chemistry C,** v. 112, n. 40, p. 15900-15907, 2008/10/09 2008. ISSN 1932-7447. Available: < http://dx.doi.org/10.1021/jp803775j >

[22] GLASSCOCK, J. A. et al. Enhancement of Photoelectrochemical Hydrogen Production from Hematite Thin Films by the Introduction of Ti and Si. **The Journal of Physical Chemistry C,** v. 111, n. 44, p. 16477-16488, 2007. Available: < http://dx.doi.org/ 10.1021/jp074556l >

[23] CRAIG A. GRIMES, O. K. V., SUDHIR RANJAN. Light, Water, Hydrogen: The Solar Generation of Hydrogen by Water Photoelectrolysis. **Springer US**. Boston, 2008. ISBN: 978-0-387-33198-0 (Print) 978-0-387-68238-9 (Online). Available: < http://dx.doi.org/10.1007/978-0-387-68238-9 >

[24] Jeffrey J. Urban, Wan Soo Yun, Qian Gu, and Hongkun Park. Synthesis of Single-Crystalline Perovskite Nanorods Composed of Barium Titanate and Strontium Titanate, **Journal of American Chemical Society**, 2002, 124 (7), pp 1186–1187. Available: < http://dx.doi.org/10.1021/ja017694b >

[25] Antonio N. Pinheiro, Edney G. S. Firmiano, Adriano C. Rabelo, Cleocir J. Dalmaschio and Edson R. Leite. Revisiting SrTiO3 as a photoanode for water splitting: development of thin films with enhanced charge separation under standard solar irradiation. **Royel society of chemistry advances.** 2014,**4**, 2029-2036. Available: < http://dx.doi.org/10.1039/C3RA45066J >

[26] Yiqing Bia,b, Muhammad Fahad Ehsana,b, Yan Huanga, Jiarui Jina,b, Tao Hea, Synthesis of Cr-doped SrTiO3 photocatalyst and its application in visible-light-driven transformation of CO2 into CH4. **Journal of CO2 Utilization.** Volume 12, December 2015, Pages 43–48. Available : < http://dx.doi.org/10.1016/j.jcou.2015.10.004 >

[27] KAKIHANA, M. Invited review "sol-gel" preparation of high temperature superconducting oxides. **Journal of Sol-Gel Science and Technology,** v. 6, n. 1, p. 7-55, 1996/01/01 1996. ISSN 0928-0707. Available: < http://dx.doi.org/10.1007/BF00402588 >

[28] Fujishima, A; Honda, K. Electrochemical Photolysis of Water at a Semiconductor Electrode. **Nature,**238, 37 - 38 (07 July 1972). Available: < http://dx.doi.org/10.1038/238037a0 >

[29] S. X. Ouyang, H. Tong, N. Umezawa, J. Cao, P. Li, Y. Bi, Y. Zhang and J. Ye, Surface-Alkalinization-Induced Enhancement of Photocatalytic H2 Evolution over SrTiO3 - Based Photocatalysts. **Journal of American Chemical Society**. 2012, 134, 1974–1977. Available: < http://dx.doi.org/10.1021/ja210610h >

[30] H. Zhao, F. Gao, X. Li, C. Zhang, Y. Zhao, **Solid State**

[31] Xue Li, Hailei Zhaoa, Wei Shen, Feng Gao, Xianliang Huang, Yue Li, Zhiming Zhu. Synthesis and properties of Y-doped SrTiO3 as an anode material for SOFCs. **Journal of PowerSources**.166(2007)47–52. < http://dx.doi.org/10.1016/j.jpowsour.2007.01.008 >

[32]http://photon-science.desy.de/research/research_highlights/archive/perovskite_ like_crystal_in_an_electric_field/index_eng.html. Access date : 16/01/2017.

[33] Wicklein, Sebastian. Defect engineering of SrTiO3 thin films for resistive switching Applications. **Deutsche national bibliothek**. ISBN: 978-3-89336-963-8 <http://d-nb.info/1054089825>

[34] R. D. LEAPMAN, L. A. GRUNES, AND P. L. FEJES, Study of the L23 edges in the 3d transition metals and their oxides by electron-energy-loss spectroscopy with comparisons to theory, **Physical Review B**, 26,614-635(1982). Available: < http://dx.doi.org/10.1103/PhysRevB.26.614 >

[35] Goldscmidt, **Geochemistry**, Oxford University press, 1958.

[36] Wells, (1995) Structural Inorganic Chemsitry, Oxford Science publications. Müller, (1993). **Inorganic Structural Chemistry**, Wiley & Sons Ltd. ISBN: 978-0-470-01864-4.

[37] Feng Gao, Hailei Zhaoa, Xue Lia, Yunfei Cheng, Xiong Zhou, Fenge Cui. Preparation and electrical properties of yttrium-doped strontium titanate with B-site deficiency. **Journal of Power Sources**. Volume 185, Issue 1, 15 October 2008, Pages 26–31. Available: < http://dx.doi.org/10.1016/j.jpowsour.2008.07.015 >

[38] Pradhan, G S Roy. Study the Crystal Structure and Phase Transition of BaTi3– A Pervoskite. **Researcher.** 2013;5(3):63-67]. (ISSN: 1553-9865). Available: < http://www.sciencepub.net.10 >

[39] T. Kolodiazhnyi, A. Petric, The Applicability of Sr-deficient *n*-type $SrTiO_3$ for SOFC Anodes. **Journal of Electroceramics,** Volume 15, Number 1, September 2005, pp. 5-11(7). Available : < http://dx.doi.org/10.1007/s10832-005-0375-7 >

[40] L. E. REHN, **Nucl. Instrum. and Methods**, B64, 161 (1992).

[41] P. Ramirez, Colossal magnetoresistance. **Journal of Physics: Condensed Matter**, 9, 8171 (1997). Available: < http://dx.doi.org/10.1088/0953-8984/9/39/005 >

[42] T. higuchi, T. Tsukamoto, N. Sata, M. Ishigame, Y. Tezuka, and S. Shin, Electronic structure of p-type SrTiO3 by photoemission spectroscopy, **Physical Review B** ,57, 6978 – 15 March 1998, Available: < https://doi.org/10.1103/PhysRevB.57.6978 >

[43] J. W. Liu, G. Chen, Z. H. Li, and Z. G. Zhang. Electronic structure of visible light photo-catalysis water splitting property of Cr doped $SrTiO_3$. **Journal of Solid State Chemistry**.179,3704–3708(2006). Available < http://dx.doi.org/10.1016/j.jssc.2006.08.014 >

[44] D. Hertkorn, H. C. Elsenheimer, R. Bruch, F. Paul, C. Müller, T. Hanemann, and H. Reinecke . Thickness variation of electrophoretically deposited strontium titanate films for photoelectrochemical energy conversion. **Journal of Applied Physics** , Volume 114, Issue 2, July 2013, Available : < http://dx.doi.org/10.1063/1.4811817 >.

[45] T. S. Wu, H. D. Li, Y. W. Chen, S. F. Chen, Y. S. Su, C. H. Chu, C. W. Pao, J. F. Lee, C. H. Lai, H. T. Jeng,S. L. Chang and Y. L. Soo. Unconventional interplay between heterovalent dopant elements: Switch-and-modulator band-gap engineering in (Y, Co)-Codoped CeO2

nanocrystals. **Scientific Reports 5**, Article number: 15415 (2015), Available: < http://dx.doi.org/10.1038/srep15415 >

[46] D. Hertkorn, M. Benkler, U. Gleißner, F. Bu¨ker, C. Megnin, C. Muller, T. Hanemann, H. Reinecke. Morphology and oxygen vacancy investigation of strontium titanate-based photo electrochemical cells. **Journal of Materials Science**, 50(1) , August 2014. Available: < http://dx.doi.org/10.1007/s10853-014-8563-y >

[47] Ryoichi FURUSHIMA, Satoshi TANAKA, Zenji KATO and Keizo UEMATSU - Orientation distribution–Lotgering factor relationship in a polycrystalline material—as an example of bismuth titanate prepared by a magnetic field. **Journal of the Ceramic Society of Japan**, Vol. 118 (2010) No. 1382 (October) P 921-926. Available: < http://doi.org/10.2109/jcersj2.118.921 >

[48] Daniel M. Cunha, Flavio L. Souza. Facile synthetic route for producing one-dimensional zinc oxide nanoflowers and characterization of their optical properties. **Journal of Alloys and Compounds**,577:158–164, November2013 < http://dx.doi.org/10.1016/j.jallcom.2013.04.126 >

[49] T. Ami and M. Suzuki: MOCVD growth of (100)-oriented CeO2thin films on hydrogen-terminated Si(100) substrates. **Materials Science and Engineering: B**, Volume 54, Issues 1–2, 12 June 1998, Pages 84–91, Available < http://dx.doi.org/10.1016/S0921-5107(98)00133-0 >

[50] André L.M. Freitas, Waldemir M. Carvalho Jr., and Flavio L. Souza. Enhanced water oxidation efficiency of hematite thin films by oxygen deficient atmosphere. **Journal of Materials Research**, Volume 30 Issue 23, December 2015, pp. 3595-3604, Available : < https://doi.org/10.1557/jmr.2015.353 >

[51] MONSHI, A.; FOROUGHI, M.; MONSHI, M. Modified Sherrer Equation to Estimate More Accurately Nano-Crystallie Size Using XRD. **World Journal of Nano Science and Engineering**,Vol.2No.3,2012,pp.154-160. < http://dx.doi.org/10.4236/wjnse.2012.23020 >

[52] Surendar Tonda,a Santosh Kumar,a Oruganti Anjaneyulub and Vishnu Shanker*a Synthesis of Cr and La-codoped SrTiO3 nanoparticles for enhanced photocatalytic performance under sunlight irradiation. **Physical Chemistry Chemical Physics**, 2014, **16**, 23819-23828, Available: < http://dx.doi.org/10.1039/c4cp02963a >

[53] Callister , willian D, 1940 – **Materials science and engineering : an Introduction** 1940, 7th ed. John Wiley & Sons, Inc. ISBN-13: 978-0-471-73696-7 (cloth) ,ISBN-10: 0-471-73696-1 (cloth).

[54] Troy K. Townsend, Nigel D. Browning and Frank E. Osterloh. Overall photocatalytic water splitting with NiOx–SrTiO3 – a revised mechanism. **Energy and Environmetal Science**, 2012,**5**, 9543-9550, Available: < http://dx.doi.org/10.1039/c2ee22665k >

[55] Toru Hara, Takashi Ishiguro, and Kazuo Shinozaki. Ultraviolet-Light-Induced Desorption of Oxygen from SrTiO3 Surfaces. **Japanese journal of Applied Physics**, Volume 50, number 4R, 20 April 2011, Available : < http://dx.doi.org/10.1143/JJAP.50. >

[56] Toru Hara, Takashi Ishiguro. Oxygen sensitivity of SrTiO3 thin film prepared using atomic layer deposition. **Sensors and Actuators B: Chemical** Volume 136, Issue 2, 2 March 2009, Pages 489–493, Available: < http://dx.doi.org/10.1016/j.snb.2008.12.026 >[57] KRISHNAN, R. Fundamentals of Semiconductor Electrochemistry and Photoelectrochemistry. In: (Ed.). Encyclopedia of Electrochemistry: Wiley-VCH Verlag GmbH & Co. KGaA, 2007. ISBN 9783527610426.

[58] Shiqiang Hui and Anthony Petric. Electrical Properties of Yttrium-Doped Strontium Titanate under Reducing Conditions **Journal of the electrochemical society** 2002 149(1): J1-J10.

[59] Willian D. Callister, Jr. **Material science and engineering: an introduction** (7th ed) ISBN-13: 978-0-471-73696-7 (cloth) ISBN-10: 0-471-73696-1 (cloth).

[60] Andreas Zuttel. Hydrogen storage methods. **Naturwissenschaften** (2004) 91:157–172 . Available: < dx.doi.org/ 10.1007/s00114-004-0516-x >.